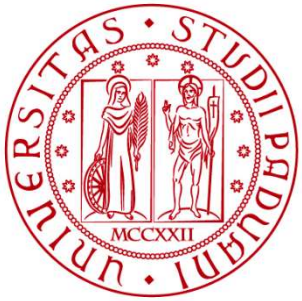

UNIVERSITÀ DEGLI STUDI DI PADOVA

Head Office: Università degli Studi di Padova

Department of Biology

Ph.D. Course in: *Biosciences*

Curriculum: *Cell Biology and Physiology*

XXXV Cycle

THESIS TITLE

Identification and characterization of signaling and axonal migration defects in the MPS II zebrafish model

Coordinator: Prof. Ildikò Szabò

Supervisor: Prof. Enrico Moro

Ph.D. student: Rosa Manzoli

INDEX

LIST OF ABBREVIATIONS

ADt: Anterior Dorsal telencephalic
AG: Axon Guidance
Arp2/3: Actin Related Protein 2/3
Ath5: Atonal homolog 5
BBB: Blood-Brain Barrier
BMP: Bone morphogenetic protein
CDC42: Cell Division Cycle 42
CDH2: Cadherin 2
ChP: Choroid Plexus
CLN1: Neuronal ceroid lipofuscinosis 1
CMM: Congenital Mirror Movement
CNS: Central Nervous System
DAG: Diacylglycerol
Dcc: Deleted in Colorectal Cancer
DIV: Day(s) *in vitro*
dpf: Day(s) post fertilization
DS: Dermatan Sulfate
EE: Early Endosome
EGF: Epithelial Growth Factor
EGFR: Epithelial Growth Factor Receptor
ELK1: ETS Like-1
ENA-VASP: Enabled/vasodilator-stimulated phosphoprotein
Eph: Ephrin
ERT: Enzyme Replacement Therapy
ESCRT: Endosomal Sorting Complexes Required for Transport
FAK: Focal Adhesion Kinase
FBS: Fetal Bovine Serum
FN: Fibronectin
GABA: Gamma-aminobutyric acid
GAG: Glycosaminoglycans
Gapdh: Glyceraldehyde-3-Phosphate Dehydrogenase
Gfap: Glial fibrillary acidic protein
GPI: Glycosylphosphatidylinositol
GTP: Guanosine Triphosphate
HIV: Hour(s) in vitro
hpf: hour(s) post fertilization
HS: Heparan Sulfate
IDS: Iduronate-2-Sulfatase
IP3: Inositol trisphosphate
ITC: Intertectal Commissure
Lamp1: Lysosomal-associated membrane protein 1
LC3: Microtubule-associated protein 1A/1B-light chain 3

LE: Late Endosome
LSD: Lysosomal Storage Disorder
MAP: Microtubule-Associated Proteins
MAPK: Microtubule-Associated Proteins Kinase
MPS: Mucopolysaccharidosis
NCK: Non-Catalytic region of tyrosine Kinase
NEO: Neogenin
NMDA: N-methyl-D-aspartate
N-WASP: Neural Wiskott-Aldrich syndrome protein
O/N: Over Night
P62: Ubiquitin-binding protein p62/ Sequestosome-1
PAK1: Serine/threonine-protein kinase
PI3K: Phosphoinositide 3 kinase
PIP2: Phosphatidylinositol-4,5-biphosphate
PIP3: Phosphatidylinositol 3,4,5-triphosphate
PKC: Protein kinase C
PLC: Phospholipase C
Rab: Ras-associated binding
RAC1: Ras-related C3 botulinum toxin substrate 1
RE: Recycling Endosome
RGC: Retinal Ganglion Cell
RGM: Repulsive guidance molecule
ROBO: Roundabout
RT: Room Temperature
Shh: Sonic Hedgehog
SNP: Single Nucleotide Polymorphism
TH: Tyrosine Hydroxylase
wt: wild type

ABSTRACT

Mucopolysaccharidosis type II (MPS II), also known as Hunter syndrome, is a rare X-linked lysosomal storage disorder caused by the lack or deficiency of iduronate 2-sulfatase (IDS), a lysosomal enzyme involved in the first step of heparan and dermatan sulfate degradative pathway. This results in a plethora of somatic and central nervous system (CNS)-related symptoms with high clinical variability and different age of onset. While enzyme replacement therapy can alleviate somatic manifestations, the CNS remains untreatable. Historically, the pathogenesis of MPSs has been attributed to the progressive intracellular accumulation of undegraded glycosaminoglycans (GAGs) and inflammation; however, it is now clear that more complex pathogenic mechanisms may contribute to the pathological manifestations, including impaired autophagy and altered developmental cell signalling.

In this context, I exploited the MPS II zebrafish model to deepen the understanding of early pathological mechanisms during brain development. In particular, I focused my research on the investigation of Netrin and Deleted in colorectal cancer (Dcc), one of the most important pair of ligand and receptors, involved in axon guidance-mediated chemoattraction. While both Netrin and Dcc showed altered expression pattern in a *in situ*-based screening, only Dcc was consistently found altered at protein levels. To this purpose, I performed western blot analysis on dissected heads and isolated brains at early developmental stages. Moreover, to scale up the resolution of my investigation, I set up an optimized protocol for zebrafish primary neuronal-enriched cell culture. This tool allowed me to narrow down Dcc dysregulation specifically to the neuronal compartment. The *in vitro* neuronal model allowed to detect alterations in Dcc downstream cascade activation, lysosomal acidification and Ras-associated binding 7 (Rab7) protein levels in mutant cells. In addition, I applied zebrafish primary neurons to a microfluidic system to dissect axonal morphology. Indeed, mutant-derived neurons showed shorter axons when compared to control cells.

Since Dcc regulation relies on vesicular trafficking, I analysed Dcc intracellular localization in the head of MPS II larvae. Toward this aim, I set up a novel protocol of fractional precipitation applied to zebrafish protein extracts that allowed me to find an altered Dcc localization in *ids* mutant conditions. Moreover, Dcc analysis at later time points highlighted a consistent dysregulation of this receptor beyond the developmental phase.

In addition, a Glial fibrillary acidic protein (Gfap) protein levels analysis revealed that pathological abnormalities are traceable since 1 month of age in MPS II zebrafish brains, suggesting early glial cell activation.

Western blot analysis of heparan sulfates (HS) showed no significant differences between wild type and *ids* mutant larvae at early developmental stages. On the other hand, whole mount brain HS immunofluorescence pointed out abnormal choroid plexus architecture in MPS II larvae.

Finally, retinotopic mapping and multiple behavioural tests based on visual stimulation suggested subtle but not significant alterations in mutant fish at larval stages.

SOMMARIO

La Mucopolisaccaridosi di tipo II (MPS II), conosciuta anche come Sindrome di Hunter, è una malattia da accumulo lisosomiale con ereditarietà legata al cromosoma X. Questa patologia è causata da mutazioni a livello del gene codificante per l'iduronato-2-sulfatasi, un enzima lisosomiale coinvolto nel primo step di degradazione di eparan e dermatan solfato. Lo spettro di sintomi che ne deriva è estremamente ampio con manifestazioni sia somatiche che legate al sistema nervoso centrale. Mentre l'approccio di terapia enzimatica sostitutiva risulta efficace nell'alleviare i sintomi di natura somatica, il trattamento del sistema nervoso centrale rimane tutt'ora di grande difficoltà. La patogenesi delle mucopolisaccaridosi è stata storicamente attribuita al progressivo accumulo di glicosamminoglicani e al conseguente instaurarsi di una condizione infiammatoria; tuttavia, è ormai chiaro che più complessi meccanismi, tra cui deregolazione della via autofagica e alterazione di vie di segnale durante lo sviluppo, contribuiscano all'insorgenza della patologia.

In questo contesto, mi sono servita del modello zebrafish per l'MPS II per studiare i meccanismi patologici precoci relativi allo sviluppo cerebrale. In particolare, la mia ricerca si è focalizzata sull'analisi di Netrin/Dcc (Deleted in colorectal cancer), una delle più importanti vie di segnale coinvolte nel processo noto come *axon guidance*. Sebbene sia Netrin che Dcc mostrassero un alterato profilo di espressione, solo Dcc si è rilevato consistentemente deregolato a livello proteico, sia nell'intera testa che nel cervello isolato di larve *ids* mutanti. L'ottimizzazione di un protocollo per colture primarie di zebrafish ha inoltre consentito di attribuire questa alterazione specificamente al comparto neuronale. Tale modello *in vitro* ha evidenziato difetti nella via di segnale regolata da Dcc, nell'acidificazione lisosomiale (Lysotracker) e nei livelli proteici di Rab7 nei neuroni derivati da *ids* mutanti. In aggiunta, con l'intento di valutare la morfologia assonale, ho applicato le colture di neuroni primari ad un supporto di microfluidica: nello specifico, ho

osservato una riduzione nella lunghezza assonale dei neuroni mutanti rispetto ai controlli.

Poiché la regolazione del recettore Dcc è strettamente dipendente dal traffico vescicolare, ho successivamente analizzato la sua localizzazione intracellulare nella testa delle larve MPS II. A tal proposito, sono stata impegnata nella messa a punto di un nuovo protocollo di precipitazione frazionata applicabile ad estratti proteici di zebrafish. Questo mi ha permesso di osservare una alterata localizzazione di Dcc a livello intracellulare nelle larve *ids* mutanti. In aggiunta, l'alterazione dei livelli di Dcc si è dimostrata un fenomeno non solo relativo ai primi stadi di sviluppo, ma anche a fasi più tardive della vita dello zebrafish.

Questo aspetto è accompagnato da anomalie nei livelli proteici della proteina acida fibrillare gliale (Gfap), rintracciabili già a partire da 1 mese di età nei cervelli di zebrafish MPS II, suggerendo un'attivazione precoce delle cellule gliali.

Per quanto riguarda l'analisi dei livelli di eparan solfato, non sono state rilevate significative differenze tra controlli sani e larve *ids* mutanti nelle prime fasi di sviluppo. Tuttavia, la valutazione tramite l'immunofluorescenza ha evidenziato, nelle larve MPS II, un'architettura anomala del plesso coroideo struttura rivelatasi arricchita di eparan solfato.

Infine, analisi retinotopiche del tetto ottico e test basati su stimolazioni visive hanno suggerito alterazioni lievi ma non significative nei pesci mutanti a stadi larvali.

INTRODUCTION

1. Mucopolysaccharidosis type II

Mucopolysaccharidosis type II (MPS II), also known as Hunter syndrome, is a rare X-linked disease belonging to the broad family of Lysosomal Storage Disorders (LSDs). These pathologies are caused by mutations in genes encoding proteins involved in lysosomal functions, whose defective activity ultimately affects organelle homeostasis leading to the gradual accumulation ("storage") of undegraded substrates. Individually, each of these disorders is rare. However, if considered all together, LSDs cumulative prevalence is relatively high (approximately 1 in 8000 live births) when compared to other groups of rare diseases (Parenti, 2009).

Among LSDs, Mucopolysaccharidoses are characterized by the deficiency of lysosomal enzymes involved in the catabolism of glycosaminoglycans (GAGs), long unbranched polysaccharides commonly found on cell membranes or in the extracellular matrix. In particular iduronate-2-sulfatase (IDS), that catalyses the first step of heparan and dermatan sulfates degradation, is the hydrolase of which mutations are implied in the MPS II onset. About 700 *IDS* pathogenic variants have been registered in the Human Gene Mutation Database, from missense mutations to gross deletions. Different types of alterations can affect the enzymatic activity with variable degrees; however it should be noticed that a higher residual activity is not directly correlated to a better prognosis (Corrêa et al., 2022). It has been reported that patients harbouring the same mutation may exhibit profoundly different clinical manifestations (Vafiadaki et al., 1998). As related to symptomatology, also the age of onset is extremely variable: in the most serious cases MPS II is already diagnosed at 12-18 months of age, while in milder forms first symptoms can appear during adulthood.

Since IDS is ubiquitously expressed, all cell types suffer from lysosomal dysfunction therefore resulting in a wide spectrum of symptoms. Based on the type of clinical manifestations, MPS II patients are classified in two groups. Patients of the *non-*

neuronopathic (*attenuated)* form display only somatic symptoms which can include hepatosplenomegaly, skeletal defects, cardiomyopathies, respiratory failure and coarse facial features. On the other hand, patients suffering from central nervous system (CNS)-related issues, in addition to somatic symptoms, are grouped as *neuronopathic (severe)*: retinal degeneration, impairment of gross and fine motor abilities, seizures-like behaviour, cognitive impairment, developmental delay and progressive neurocognitive regression are only some of the features of the severe forms (*Fig. 1*) (Barone et al., 2018).

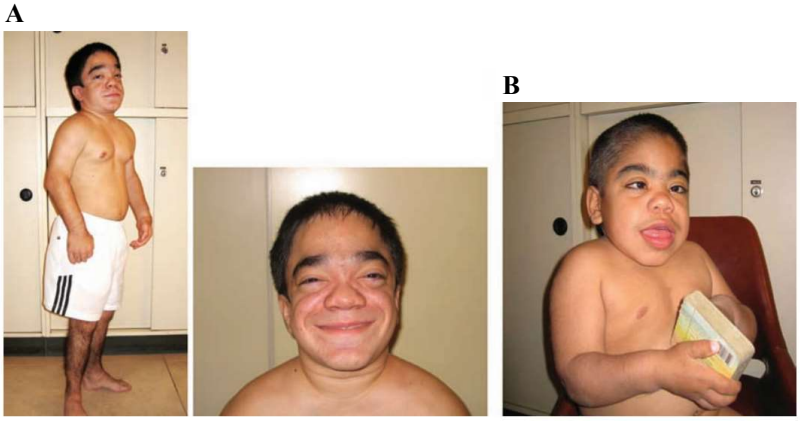

Fig. 1. MPS II patients. (A) *A 19 years old patient suffering from MPS II attenuated form and showing skeletal abnormalities and posture defects. The typical facial features of MPS II patients including prominent forehead, broad nose with a flattened bridge and wide mouth are depicted in the magnified picture.* ***(B)*** *A 5 years old patient with neuronopathic Hunter syndrome (adapted from Amartino, 2015).*

Different therapeutic approaches have been proposed for the treatment of Mucopolysaccharidoses, from gene therapy to hematopoietic stem cell transplantation, but targeting the central nervous system remains challenging. Indeed, the only available therapy is represented by the enzyme replacement therapy (ERT) that is not able to alleviate neurological manifestations due to the enzyme inability to cross the blood-brain-barrier (BBB). Intrathecal infusion is the only way ERT can reach the central nervous system, but with the drawback to be a highly invasive and risky approach. In the latest years, a new version of the enzyme has been approved for MPS treatment in Japan: in this novel formulation, called *Pabinafusp alfa*, recombinant-IDS is fused with a humanized anti-human transferrin receptor antibody that allows IDS delivery, by transcytosis, to the brain

parenchyma upon intravenous administration (Morimoto et al., 2022). However, the lack of long-term studies concerning its safety make the understanding of MPS II neuropathogenesis highly demanding.

For many years, the organ dysfunctions have been attributed to lysosomal accumulation of undigested substrates. However, recent evidence have pointed out that, even before lysosomal engorgement, autophagic flux and signaling pathways are impaired in MPS (Fiorenza et al., 2018; Myerowitz et al., 2021). This is supported by the fact that correct lysosomal function is not only required for substrate degradation, but it also affects cell membranes composition, vesicles trafficking, mitochondrial homeostasis, oxidative stress, regulation of signaling pathways and inflammation (Fecarotta et al., 2020).

1.1 Neuronopathic MPS II

MPS II neurological phenotype is highly variable both in the age of onset and in type of manifestations, from mild and slowly progressing cases to most severe ones with a very rapid development. CNS-related signs can be detected by 4 years of age, but they can be anticipated to 12 months in the most severe forms. Regardless of the timing, CNS-related symptoms are extremely life-threatening for paediatric patients and reflect in a huge distress in their families, having a disruptive impact on the quality of life of both children and parents. In 2020, Eisengart and colleagues conducted a complex multi-faceted study in which they recapitulated the recurrent clinical manifestations of neuronopathic MPS II patients. According to this study, children display low attention level and high distractibility, hyperactive and impulsive behaviours characterized by constant moving. Since their persistent seek for sensory inputs, children's behaviour can be mistaken for aggressiveness; moreover, their inability to manage emotional expression, with sudden outbursts of emotions without a clear trigger, is usually ascribed to an "autism-like" phenotype (Eisengart et al., 2020).

Behavioural manifestations are frequently reflected by anatomical abnormalities of the CNS. MPS II patients may present focal or diffuse white matter lesions that can worsen with ageing. It is supposed that these lesions, mirroring a gliosis status,

derive from the delay of myelination in young children and progressive demyelination observed during ageing. One of the most frequently affected structure of the brain is the corpus callosum, a thick fascicle of commissures enabling left and right hemispheres communication. Brain lesions are also accompanied by hydrocephalus and atrophy in MPS II due to cerebrospinal fluid reabsorption failure and progressive neuronal death, respectively (Palmucci et al., 2013). As previously mentioned, astrocytes and microglial activation is suggested to have an impact on MPS pathogenesis. Neuronal altered homeostasis and death, oxidative stress, astrocytic dysfunction and pro-inflammatory cytokines release are phenomena sustaining one another leading, at the end, to the self-perpetuating detrimental neuroinflammatory state (Bosch and Kielian, 2015).

In this context and since ERT is highly ineffective in treating CNS manifestations, the understanding of the pathological basis underlying the central nervous system manifestations in neuronopathic MPS is recognized to be crucial. In fact, not only it allows to develop novel and targeted therapies, but it also can lead to the identification of specific biomarkers fundamental for early diagnosis and monitoring of disease progression (Viana et al., 2020).

2. Modelling MPS II in vivo

2.1 Canine model

The first animal model for MPS II was described in 1998 with the case of a 3 years old Labrador Retriever initially examined for incoordination (Wilkerson et al., 1998). This was a spontaneous and isolated MPS canine model since the affected animal did not generate offspring. Further analyses revealed that, in addition to incoordination, the MPS dog also displayed asymmetric ataxia and paresis of the limbs, corneal defects, hepatosplenomegaly, osteopenia of the axial skeleton, coarse facial features and tongue enlargement, thus resembling some of the human symptoms.

2.2 Murine model

The first MPS II mouse model was generated by Muenzer and colleagues in 1999: this line harbours, in the *Ids* sequence, a deletion of exon 4 and part of exon 5 thus resulting in a null mutation (Muenzer and Fu, 1999). An extensive characterization of this *Ids* mutant strain (Garcia et al., 2007) has allowed to identify some characteristic features that are summarized in the following list:

- Reduced lifespan: 1 year compared to 2,5 years of wild type littermates;
- Coarse fur and sporadic alopecia by 10 weeks of age, together with gibbous deformities in hind limb articulation and impaired joint mobility (ankylosis). Curved position, broadened snouts, smaller body size when compared to healthy littermates (*Fig. 2*);
- Skeletal deformities including abnormal skull development displaying bone enlargement by 4 weeks of age; abnormal calcification of the calcaneus tendon at 48 weeks;
- Organomegaly: at 7 weeks of age high concentration of GAGs are seen in liver, spleen, kidney, skin, lung, brain and heart. GAG levels remain dysregulated throughout the entire life.

Fig. 2. MPS II knockout mouse model. (A) *Wild-type mouse of 9 months of age compared to age matched MPS II mouse model* ***(B)****. the IDS-knockout mouse phenotype progressively worsens with coarse fur, broadened snouts and enlargement of the skull bones as shown in* ***(C)****. Adapted from Muenzer and Fu 1999.*

Concerning the CNS, MPS II mice show hyperdopaminergia at the level of substantia nigra (De Risi et al., 2021), as well as increased marker of neuroinflammation at early stages (8 days). The neuroinflammatory phenotype seems to precede glial degeneration, which becomes evident only by 6 weeks of age and consistently present also at 6, 8 and 11 months (Motas et al., 2016; Zalfa

et al., 2016). This inflammatory condition inevitably leads to neurodegeneration, thus resulting in neuronal necrosis of brainstem and spinal cord by 60 weeks of age (Garcia et al., 2007; Polito and Cosma, 2009). Furthermore, a bulk RNA sequencing of MPS II mice brain at 9 months has pointed out significant variations in the expression of proteins implicated in fundamental biological processes, such as calcium signaling, synapses communication and axon guidance (Salvalaio et al., 2017).

To assess whether the mouse model also recapitulated the behavioural component of the disease, numerous tests have been performed. While no differences have been reported in sociability trials (Gleitz et al., 2017), changes in anxiety-related behaviour and locomotor activity have been detected between 36 and 40 weeks of age (Cardone et al., 2006), together with significant changes in long-term memory (Hinderer et al., 2016).

2.3 Zebrafish model

Zebrafish (*Danio rerio*) is a teleost belonging to the *Cyprinidae* family. Its role as a versatile model organism has been proposed since the '80s and nowadays it is one of the most widely used models in laboratory practices. External fertilization, optical clarity and rapid development are only some of the most known advantages of this small fish. Furthermore, these features allow to perform non-invasive live imaging, such as brain activity recording. Given its high fecundity and the chance to test a considerable number of animals, zebrafish is also widely used in behavioural assays. The possibility of monitoring embryonic maturation in real time make zebrafish an extremely appealing model for developmental studies. In this context, it's not surprising that Ids involvement in first developmental mechanisms was demonstrated precisely in the zebrafish model. Indeed, in 2010 Moro and colleagues showed that *ids* knockdown leads to impaired embryonic anterior–posterior patterning and cartilages maturation (Moro et al., 2010). In addition, a later investigation revealed that loss of Ids function generates defects in cardiac cell differentiation and atrioventricular valve formation (Costa et al., 2017).

Moreover, the availability of well-established mutagenesis tools applicable to the zebrafish organism allowed the generation of a stable *ids* mutant zebrafish through CRISPR/Cas9 technology. The mutant is characterized by a 5 base pair deletion within *ids* exon2 (chr14), causing a frameshift in the reading frame and the generation of a premature stop at codon 118: this leads to the translation of a non-functional Ids protein (Bellesso et al., 2018). *ids* mutant larvae display early developmental defects including impaired migration and differentiation of neural crest cells into chondroblasts, together with a dysmorphic skeleton (*Fig. 3*) and hepatomegaly thus resembling some of the human symptoms.

While some MPS II somatic manifestations have already been characterized in the zebrafish model, no CNS-related defects have been investigated yet.

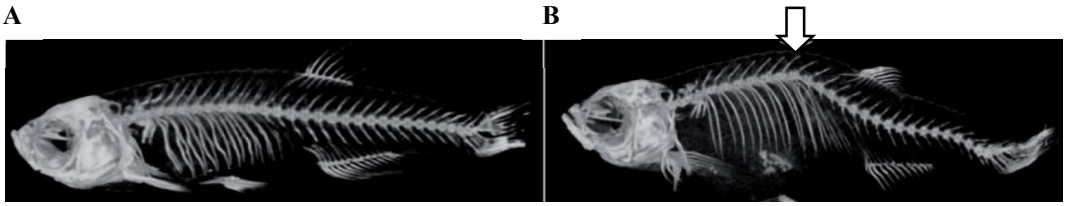

Fig. 3. MPS II knockout zebrafish model. *3D reconstruction of a* ***(A)*** *Wild-type 15 months old fish compared to* ***(B)*** *age matched ids knockout. The MPS II zebrafish model display evident skeletal abnormalities at the level of the backbone (white arrow)* (adapted from Bellesso et al., 2018).

3. Axon guidance

During CNS development, axons extend towards their targets by exploring the surrounding environment. This process is directed by the growth cone, a dynamic structure placed at the axonal tip. Since the distances can be very long, axons need to be precisely guided. For this reason, all the mechanisms involved in this critical developmental phase are altogether referred as *axon guidance* (AG). The whole process results in the formation of specific and predictable paths due to the interplay of a huge variety of molecules, from morphogens (Shh, Wnt, Bmp) to chemotactic factors among which are listed both chemo-attractants and repellents. These molecules can exist both in a soluble and a membrane-bound form to mediate, respectively, long- or short-range effects.

Canonical AG-related proteins have been divided in five groups: Semaphorins, Ephrins, Repulsive guidance molecule, Slits and Netrins.

- *Semaphorins*: secreted, membrane-bound or surface attached, can mediate both attraction and repulsion through the Plexin receptors. Semaphorin-mediated signaling signal can be modulated also by integrins and proteoglycans (Cho et al., 2012; Pasterkamp et al., 2003);
- *Ephrins (Ephs)*: can be GPI-anchored or transmembrane ligands, recognized by Eph receptors. Since they are anchored ligands, their signal can be transduced only at cell-cell contacts sites; for this reason, they become fundamental in axon choice points, where axons select between two alternative routes. Originally ascribed as chemorepellents, later evidence showed Ephrins contribution also in attractive mechanisms. They have been discovered as modulators of axon guidance during retinotopic mapping (Cheng et al., 1995);
- *Repulsive guidance molecule (RGM)*: Glycosylphosphatidylinositol (GPI)-anchored glycoprotein, interacts with Neogenin (NEO) and acts as a repulsive signal. Historically described in visual system development (Monnier et al., 2002) it is also involved in the modulation of inflammatory processes taking place during the onset of autoimmune encephalomyelitis;
- *Slits*: secreted molecules involved in repulsive signaling; their pathway is mediated by roundabout (ROBO) receptor family. Slit-Robo interaction can be modulated by heparan sulfate proteoglycans (Fukuhara et al., 2008);
- *Netrins*: found both as membrane anchored (GPI) or secreted proteins. Netrins can mediate both chemoattraction through deleted in colorectal cancer (DCC) receptor binding, or repulsion when recognized by UNC receptor family.

AG pairs of ligands and receptors are not exclusive, but they are known to act through combinatorial mechanisms (Manzoli et al., 2021). Indeed, axon guidance cue crosstalk, both in time and space, is essential for proper shaping of axon-related molecular pathways (*Fig. 4*).

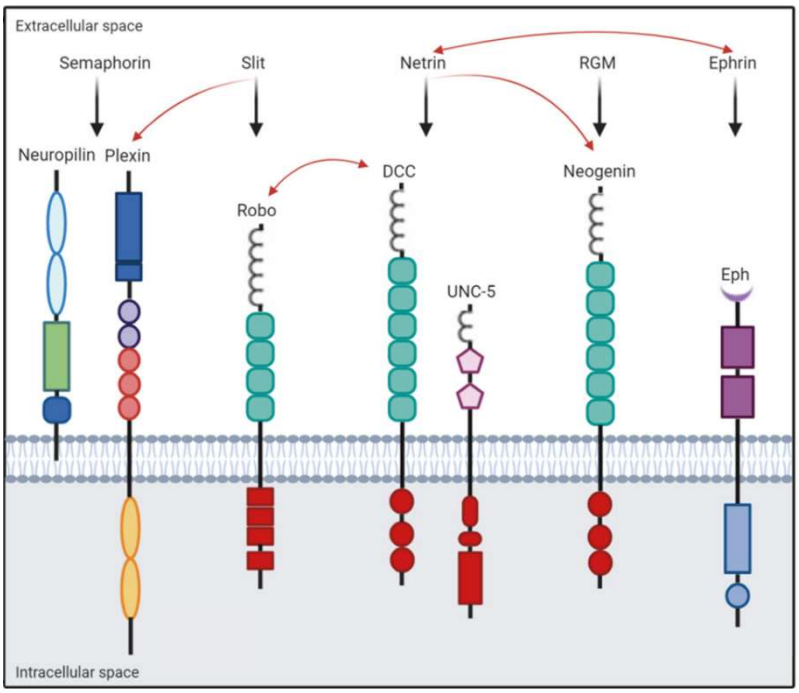

Fig. 4. Main axon guidance families of ligands and receptors*. This schematic representation depicts AG cues and receptors: black arrows stand for canonical interactions while red arrows indicate crosstalk between different axon guidance classes (adapted from Manzoli et al., 2021).*

Axonal migration is a very complex phenomenon not only involving neurons but also related to supporting cells of the developing nervous system, such as glia. In fact, it is known that glial cells can act as guidepost along migratory routes creating cellular boundaries, as “no-go” zones. This vital activity can take place through direct axon-glia interaction or glia can indirectly guide axons by shaping the extracellular microenvironment (Rigby et al., 2020). Furthermore, defects in glial development and positioning have been demonstrated to negatively affect axon pathfinding and midline crossing in the commissural tract (Sepp et al., 2001).

4. The Netrin and DCC axis

4.1 Structures and role in human diseases

Netrin/DCC pathway, one of the main axes involved in chemoattraction, has been historically studied in spinal cord development (Junge et al., 2016): floor plate Netrin attracts DCC expressing axons to the midline inducing commissural crossing.

First described in *Caenorhabditis elegans* in the early '90s (Hedgecock et al., 1990), Netrins (from Sanskrit "*Netr*" meaning '*guide*') are a family of laminin-related proteins that can be both secreted and GPI-anchored (Netrin-G). Specifically, mammals possess three diffusible (1,3 and 4) and two membrane tethered Netrins (G1 and G2). From a structural point of view, Netrins are composed by two domains at the amino-terminal: domain VI is globular while domain V is composed of three epidermal growth factor (EGF) repeats. These domains are involved in the recognition and binding to Netrin receptors. On the other side, the C-terminus is enriched in basic amino acids (*Fig. 5*) (Rajasekharan and Kennedy, 2009). Traditionally related to axon guidance, they have been shown to regulate also neuronal precursor cell migration, axon branching, synaptogenesis and oligodendroglia maturation (Lai Wing Sun et al., 2011).

On the other hand DCC, one of Netrin receptors, is a single pass transmembrane protein consisting of a long extracellular tail and a shorter cytosolic sequence of about 350 residues. The extracellular portion is composed by four immunoglobulin repeats linked to six fibronectin-like domains (FN1-FN6). This latter region is the one involved in the binding with VI/V Netrin domains. Intracellularly, DCC contains three highly conserved motifs named P1, P2 and P3 that function as docking site upon Netrin-induced receptor activation (*Fig. 5*) (Lai Wing Sun et al., 2011; Xu et al., 2018).

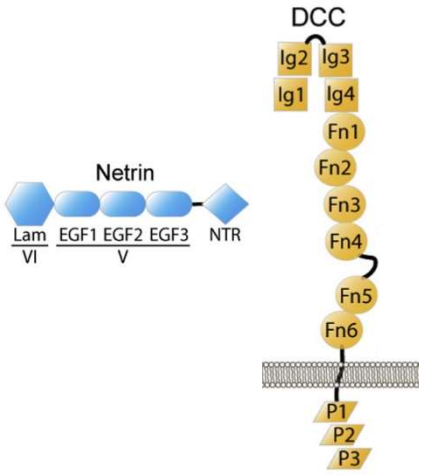

Fig. 5. Structural representation of Netrin and its receptor DCC. *Secreted Netrins are characterized by a laminin domain (VI), three EGF repeats (domain V) and a C-terminal domain named NTR. The extracellular N-terminus of DCC presents immunoglobulin repeats followed by six fibronectin domains; P1, P2 and P3 motifs compose the intracellular portion of the receptor (adapted from Meijers et al., 2020).*
Lam: laminin; EGF: epidermal growth factor; Ig: immunoglobulin; Fn: fibronectin

X-ray crystallography performed by Finci and colleagues (Finci et al., 2014) revealed that Netrin-1 C-terminus can interact with heparan sulfate and that this bond is involved in DCC dimerization and initiation of the signaling cascade (Rajasekharan and Kennedy, 2009). Moreover it has been shown *in vivo* that glypican, a heparan sulfate proteoglycan, can bind directly to DCC modulating Netrin-dependent chemoattraction (Blanchette et al., 2015).

Correct assembly of brain circuits mediated by axon guidance cues is crucial for the physiological neural activity. Indeed, it has been demonstrated that several human neuropathologies are associated with mutations in AG-related molecules. For example, the Congenital Mirror Movement (CMM) and Developmental split-brain Syndrome have been associated to DCC mutations, leading to defects in the axons of the cortico-spinal tract, partial agenesis of the corpus callosum and anomalies in commissures fasciculation; this results in severe neurological symptoms, such as intellectual disabilities and cognitive impairment (Manzoli et al., 2021). Recently, DCC and Netrin-G1 single nucleotide polymorphisms (SNPs) have been proven predictive of Parkinson's disease suggesting that, even during a prodromic stage of the disease, AG-related mechanisms could be negatively affected (Lin et al., 2009).

4.2 Netrin/DCC-mediated chemoattraction: signaling cascade

Netrin/DCC pathway activation is a complex event that involves the formation of different protein complexes and therefore needs to be precisely orchestrated.

In resting conditions, the DCC intracellular domain is bound to a non-catalytic region of tyrosine kinase (NCK1), an adaptor protein, and to a focal adhesion kinase (FAK). On the other hand, when Netrin binds DCC at the fibronectin-like domains, a complex intracellular signaling is initiated by DCC dimerization via P-3 luminal domain. The main downstream pathways are the following (*Fig. 6*) (Lai Wing Sun et al., 2011):

- *FAK-dependent pathway*: one of the first events triggered by DCC dimerization was shown to involve the interaction of the DCC-P3 motif with FAK. This bond mediates FAK conformational changes leading to kinase domain exposure and consequent FAK autophosphorylation at Tyr397 (Xu et al., 2018). Tyr397 phosphorylation constitutes the docking site for FYN, a Src tyrosine kinase, which in turns phosphorylates FAK and DCC, inducing Ras-related C3 botulinum toxin substrate 1 (RAC1) and cell division cycle 42 (CDC42) Rho GTPase activation. p21-activated kinase (PAK1) is then recruited to link NCK1 to CDC42 and RAC1, together with Enabled/vasodilator-stimulated phosphoprotein (ENA-VASP) and neuronal Wiskott-Aldrich syndrome protein (N-WASP) to induce cytoskeletal remodelling. Indeed, N-WASP binds to Actin Related Protein (Arp2/3) and induces actin filaments polymerization and growth cone orientation (Ren et al., 2004; Shekarabi et al., 2005; Li et al., 2004; Xu et al., 2018);
- *Microtubule-Associated Proteins Kinase (MAPK) cascade*: leads to ETS Like-1 (ELK1) transcription factor activation, thus affecting gene transcription (Campbell and Holt, 2003; Ma et al., 2010);
- *Phosphatidylinositol-4,5-biphosphate (PIP2) pathway*: DCC activation stimulates increased PIP2 synthesis and subsequent phosphorylation by Phosphoinositide 3 kinase (PI3K) for the final production of phosphatidylinositol 3,4,5-triphosphate (PIP3). PIP2 is also hydrolysed by Phospholipase Cγ (PCLγ) in Diacylglycerol (DAG) and Inositol trisphosphate

(IP3) leading to Protein kinase C (PKC) activation and Ca2+ release from intracellular stores (Ming et al., 1999; Xie et al., 2006).

All these pathways should be considered as interconnected mechanisms rather than independent routes. In fact, it is known that FAK clustering is stabilized by calcium influx and promoted by PIP2 increasing levels (Xu et al., 2018).

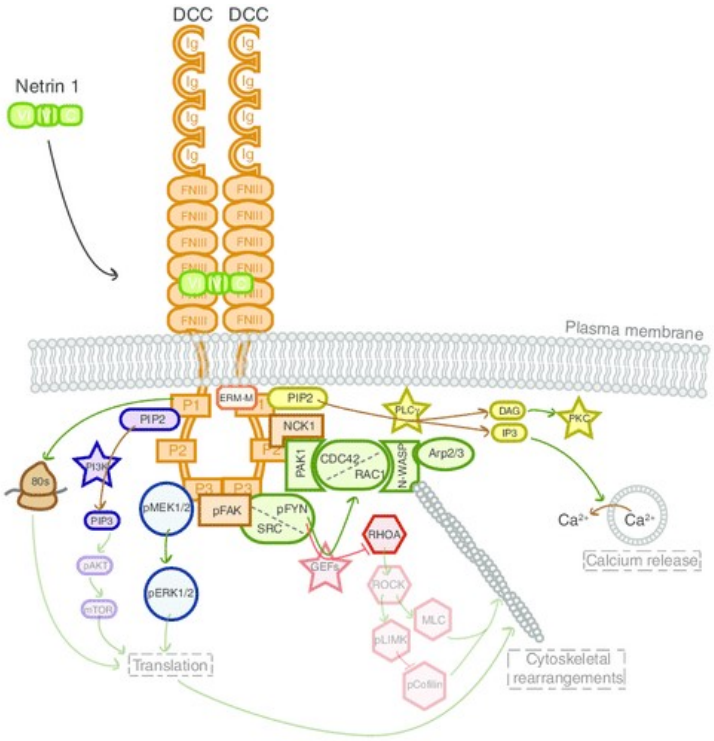

Fig. 6. Netrin/DCC downstream signaling. *Netrin binding to DCC induces receptor dimerization mediated by P3, one of DCC intracellular domains. This leads to activation of multiple signaling cascades, such as the ones related to MAPK, PIP2, FAK and Rho GTPases, resulting in cytoskeletal remodelling, calcium release and growth cone turning (adapted from Lai Wing Sun et al., 2011).*

4.3 Endocytic pathway and DCC trafficking

Growth cone dynamics are fundamental for correct axonal extension. In this context, endocytosis and exocytosis are critical processes able to modulate growth cone response to attractive or repulsive extracellular cues. Turning towards an attractive gradient, for example, needs plasma membrane expansion in the direction of the movement as well as membrane reabsorption at the opposite side (Tojima and Kamiguchi, 2015). Moreover, insertion of receptors in the membrane must be precisely regulated in time and space to mediate the correct signal inside the neuron. For this reason, receptors experience an intense shuffling between intracellular vesicles and plasma membrane. All these movements are overseen by the endocytic pathway: this system is essentially composed by vesicles derived from the plasma membrane that bud and mature thanks to Clathrin coats, Rab GTPases and ESCRT (endosomal sorting complexes) required for complexes transport. Once internalized, the endocytosed material can be recycled back to the plasma membrane inside the recycling endosomes (RE) or go through the early (EE) and then late endosomes (LE) to be delivered to the lysosome for degradation (Lamb et al., 2013). Each vesicular compartment can be identified by specific and multiple Rab proteins: for example, Rab11 is generally used as a marker for RE while Rab5 and Rab7 identify EE and LE, respectively. Being the host compartment for sorting signals, endosomes can take part in the axonal guidance-related signaling cascades (Pasterkamp and Burk, 2021).

Concerning DCC trafficking, it is known that in basal conditions DCC is dynamically inserted and removed from the growth cone membrane. On the other hand, Netrin-induced stimulation stabilizes DCC pool at the plasma membrane preventing its recycling. However, it is the activation of the downstream pathway that significantly boosts DCC insertion in the plasma membrane: the massive mobilization of DCC from its vesicular pool and its fusion with the membrane of the growth cone potentiates the membrane pool, leading to an amplified Netrin-induced response (Bouchard et al., 2004; O'Donnell et al., 2009). Once the signaling has been properly activated, DCC is once again rapidly endocytosed: co-localization with Rab11, Rab5 and Rab7 markers suggests that this receptor can be

either recycled or degraded by the endo-lysosomal pathway (Pasterkamp and Burk, 2021). Plooster and colleagues demonstrated that, in absence of proper stimulation, DCC can be ubiquitinated inhibiting the initiation of the downstream pathway and hampering vesicle fusion (Plooster et al., 2017). This suggests an additional regulation of DCC clustering on the plasma membrane by the ubiquitin-system.

Since endosomal trafficking is strictly related to lysosomal activity, any impairment of the lysosomal homeostasis can be potentially deleterious. In fact, it has been shown that primary neurons from a Krabbe disease mouse show defects in the early steps of endocytosis (Teixeira et al., 2014). The same dysregulation was also confirmed by Rappaport and colleagues using an *in vitro* model for some LSDs such as Niemann-Pick, Fabry and Gaucher disease (Rappaport et al., 2016). Receptor trafficking alterations can be equally dangerous when leading defects in the activation of the downstream pathway. In fact, mutations of WDR81, a known regulator of endosomal maturation, cause delayed epidermal growth factor receptor (EGFR) endosomal trafficking and reduced activation of the MAPK signaling pathway in radial glia progenitors, thus resulting in severe microcephaly (Carpentieri et al., 2022).

4.4 Netrin/Dcc in murine and zebrafish models

Netrin/Dcc pathway has been extensively studied *in vivo* given its implications during embryonic development and the role it plays during adulthood.

To unravel Netrin and Dcc primary functions, knock out mouse models have been generated since late '90s. Specifically, constitutive *Dcc* knockout mice display perinatal lethality therefore pointing out an indispensable role of DCC in newborn survival (Fazeli et al., 1997). Moreover, *post-mortem* analysis on $Dcc^{-/-}$ newborn mice revealed a reduction in the total number of tyrosine hydroxylase (TH)-positive cells in ventral midbrain nuclei, together with a significant increase in dopaminergic neurons migration defects and excessive axon arborization (Xu et al., 2010).

On the other side, constitutive loss of Netrin1 function results in an even more drastic phenotype with mice displaying lethality by embryonic day 14.5. These mice show severe neurodevelopmental defects associated with aberrant commissures formation at the level of the spinal cord (Bin et al., 2015).

In addition, NETRIN/DCC pathway has been found fundamental in optic nerve development (Deiner et al., 1997). Indeed, Vigouroux and colleagues demonstrated that eye-specific *Dcc* mutant mice display both severe optic nerve hypoplasia and axon pathfinding defects in the visual system (Vigouroux et al., 2020).

Even if not belonging to mammalians, the zebrafish model has been largely exploited in AG-related studies. In fact, general zebrafish brain regionalization and neuronal/glial cellular diversity are not different from the ones seen in the murine counterpart or even in humans (*Fig. 7*) (Jurisch-Yaksi et al., 2020) and it also shows equivalent synaptic structures and function (Adams and Kafaligonul, 2018). These aspects, together with its very rapid development, make the zebrafish model extremely suitable for neurodevelopmental-related studies.

Indeed, zebrafish CNS specification starts with the beginning of the gastrulation stage (6 hours post fertilization, hpf); forebrain, midbrain, and hindbrain are broadly defined already by 24 hpf and can be easily distinguished by visually identifiable morphogenetic boundaries (*Fig. 7*) (Vaz et al., 2019).

Zebrafish neurogenesis has traditionally been separated in two distinct processes, named primary and secondary neurogenesis. Primary neurogenesis refers to phenomena taking place before 2 days post fertilization (dpf): in this phase, scaffolds of transient neurons are arranged and can mediate spontaneous movements (coiling) inside the corion, the envelope surrounding the embryo. These structures are used as a guide for the addition of developing neurons by the hatching phase, finally leading to the formation of brain parenchyma (secondary neurogenesis). By 4 dpf, the nervous system is mature and larvae start displaying visual-induced behaviours. At 5-6 dpf the tectum-dependent complex behaviours such as prey-capture are shown; moreover, tectal neurons are now responsive to

visual simulation of specific size and orientation (Boulanger-Weill and Sumbre, 2019).

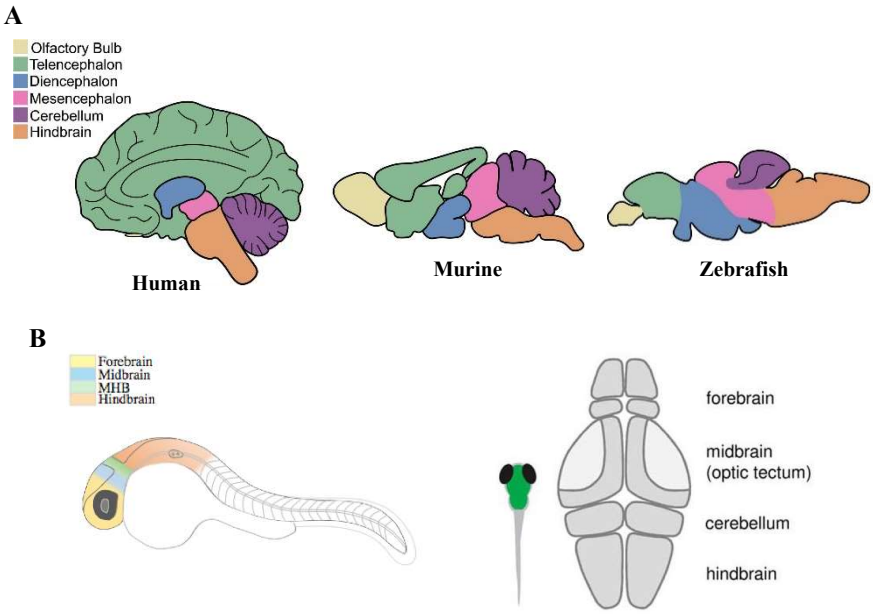

Fig. 7. Zebrafish brain organization and comparison with mammalian ones. (A) *Schematic representations of a human, murine and zebrafish brains; even if organization and sizes vary among different species, mammalians and zebrafish share similar brain anatomy and regionalization.* ***(B left)*** *Scheme of a 30 hpf zebrafish larva; different colours highlight brain main compartments already present at this embryonic stage (forebrain, midbrain and hindbrain).* ***(B right)*** *By 5-6 dpf the zebrafish is mature; the scheme depicts the main anatomical regions detectable from a dorsal view (adapted from Haynes et al., 2022; Liu and Baraban, 2019; Vaz et al., 2019)*

First studies reporting zebrafish as a model organism for axon guidance-related studies date back to the '90s. Since then, a remarkable literature has been produced concerning the role of AG-related molecules in the modulation of axonal development and regeneration.

Lauderdale in 1997 and then Hjorth in 2001 first analysed, respectively, *netrin1a* and *dcc* expression pattern in the developing zebrafish CNS by *in situ* hybridization (Hjorth et al., 2001; Lauderdale et al., 1997). While *dcc* has a unique homologue in zebrafish, *netrin 1* is present in two different isoforms, *netrin*1a and 1b. *Netrin1a* expression is traceable from 15 hpf in the embryonic CNS with high expression levels in the brain and in the ventral retina in the portion of the optic stalk, where retinal ganglion cell axons are concentrated to exit the eye and fasciculate as the optic nerve. The onset of *netrin1a* transcription is prior and concurrent with early

axonogenesis in the brain. Double staining with acetylated tubulin, a commonly used marker for neurons and axons, revealed that *netrin1a* expression domains are placed at the borders of some of the most important commissures and axonal tracts (Lauderdale et al., 1997). On the other hand, *dcc* expression pattern at early developmental stages (16-24 hpf) has been reported to correspond to the region of first neuronal clusters (Hjorth et al., 2001). Netrin/Dcc pathway is also known to participate in the development of the dopaminergic tract of zebrafish brain, together with heparan sulfate and Robo/Slit pathway, one of the most known chemorepulsive axis. Indeed, *netrin1a* and *dcc* knockdown in *robo* mutant larvae partially rescues the axonal trajectories defects of the longitudinal dopaminergic tract of the hindbrain, suggesting that Netrin/Dcc and Robo/Slit pathways work synergistically in axon guidance (Kastenhuber et al., 2009). The same cooperation is also seen in the axonal patterning of the anterior dorsal telencephalic neurons. Morpholino-based knockdown have shown that *dcc* reduced levels leads to abnormal dorsal extension of the anterior dorsal telencephalic (ADt) axons. The same dysregulation is induced by *netrin1* knockdown, in addition to abnormal ipsilateral deviation of the axonal tracts towards the supraoptic tract resulting in anterior commissure hypoplasia (Zhang et al., 2012). Recently, it has been reported that both Dcc and Netrin1 have a role in the developing olfactory bulb. In particular, knockdown of both ligand and receptor induces sensory axon misrouting (Dang et al., 2022).

Zebrafish larvae bearing mutated *dcc* exhibit defects in startle response resembling the human phenotype of the mirror movement syndrome. Defects in commissural crossing at the hindbrain level have been proposed to evoke abnormal startle response in *dcc* mutant larvae when compared to age-matched controls (Jain et al., 2014).

Now it is well established that Netrin/Dcc play additional roles beyond axon guidance, including the modulation of connectivity related processes such as axon arborization, synapse formation and maturation. In addition, even after the developmental program has been completed, this axis still retains a vital role in brain maintenance. Netrin-1 silencing in the substantia nigra of adult mice is

indeed correlated with dopaminergic loss due to DCC cleavage and consequent initiation of a cell death program (Jasmin et al., 2021; Mehlen et al., 1998). Moreover, the forebrain of adult *Dcc* conditional knockout mice exhibits altered dendritic hippocampal spines morphology, NMDA (N-methyl-D-aspartate) receptor subunits imbalance and defective hippocampal-dependent spatial memory (Horn et al., 2013). This is confirmed by analysis of mice bearing DCC haploinsufficiency: not only they display defects in the development of dopaminergic neurons, but they also show alterations in dopaminergic transmission and dopamine-related behaviour in adulthood (Vosberg et al., 2020). Finally, Netrin1-Dcc pathway has been also associated with regeneration phenomena: in nerve injury, Netrin produced by Schwann cells can act on the growth cone of the regenerating axon expressing *dcc* to direct it across a nerve gap. In the zebrafish model, *netrin1b* is expressed in Schwann cells after motor nerve transection (Dun and Parkinson, 2017). Lastly, Netrin-1 has been found important in neuroinflammation modulation by blockage of gamma-secretase processing of amyloid precursor protein (APP) (Spilman et al., 2016).

AIM OF THE THESIS

The accumulation of undegraded substrates has been always considered the main pathogenic mechanism in all lysosomal storage disorders, including Mucopolysaccharidoses. Nonetheless, the fact that patients harbouring the same genetic mutation can exhibit profoundly different symptoms with different age of onset recently led to the hypothesis that "accumulation" might not be the only leading cause of lysosomal storage disorders. Indeed, increasing evidence have shown that, even before substrates accumulation, lysosomal dysfunction can impact on cell homeostasis. Lysosomes are not only the degradative compartment of the cell, but they play a key role in vesicular trafficking, regulation of mitochondrial function and extracellular pathway modulation. Recently, an RNA-seq analysis performed on MPS II mouse brains reported dysregulation of a plethora of signaling pathways involving calcium levels, synapse receptors, cytoskeleton modulation, autophagy, oxidative stress and axon guidance molecules. Moreover, *ids* knockdown has been reported to impinge on developmental mechanisms since embryonic stages in the zebrafish model. In addition, the MPS II mouse model showed neuroinflammatory cytokines at few weeks of ages, highlighting early brain dyshomeostasis.

Starting from this evidence, the main aim of my research was to deepen the understanding of early pathological abnormalities in the brain development of a MPS II zebrafish model, particularly focusing on the axon guidance (AG)-related molecules. Indeed, not only AG cues and receptors are involved in the activation of a variety of intracellular cascades but also rely on efficient vesicular trafficking and lysosomal activity to be finely tuned. Furthermore, AG molecules such as Slit-Robo and Netrin-Dcc have been found to interact with heparan sulfates to strengthen ligand-receptor binding and enhance downstream pathway activation. Moreover, given the lack of knowledge concerning the timing of glial cell activation in the zebrafish MPS II model, I sought to investigate Gfap protein levels from early developmental stages to adulthood in the zebrafish brain. Indeed, glial cells homeostasis is fundamental during development and astrocytes activation is

generally used as a marker of neuroinflammation, one of the main features listed among MPS II symptoms.

Finally, I wanted to describe whether MPS II zebrafish larvae could display early behavioural abnormalities, in particular those triggered by visual stimulation. Visual integration is, in fact, highly dependent of proper neural circuit formation which is related to AG molecules.

MATERIALS AND METHODS

1. Animal husbandry and zebrafish manipulation procedures

All mating procedures were set up at the Fish Facility in the Department of Biology of the University of Padova. Zebrafish larvae were kept up to 5 days post fertilization (dpf) in Petri dishes with fish water (60 mg of Instant Ocean, cat. no. SS15-10, per litre of distilled water) at neutral pH at 28°C, according to standard procedures (http://ZFIN.org). All animal manipulation procedures were conducted according to the Local Ethical Committee at the University of Padova (OPBA) and National Agency (Italian Ministry of Health). The manual removal of fish chorion was performed at 24 hours post fertilization (hpf) to allow better larvae manipulation; at 24 hpf embryos were also treated, when needed, with 1-phenyl 2-thiourea (PTU) which prevents pigmentation by blocking all tyrosinase-dependent steps in the melanin pathway. This latter treatment enables to keep larvae transparent allowing better visualization of probes, transgenes and staining dyes. zebrafish were euthanized through prolonged immersion in fish water with high tricaine concentration (tricaine overdose).

2. Zebrafish lines

2.1 *ids* mutant zebrafish line ($ids^{ia200/ia200}$)

The *ids* mutant zebrafish line was previously established by Bellesso and colleagues (Bellesso et al., 2018). Briefly, the mutant harbours a 5 base pair deletion within *ids* exon2 (chr14), causing a frameshift in the reading frame and the generation of a premature stop at codon 118; this leads to the translation of a non-functional Ids protein.

2.2 Ath5-GCaMP6s

Ath5-GCaMP6s larvae were used for tectal neuropil imaging. This transgenic line was kept in Tupfel long fin nacre (TLN) background carrying a mutation

suppressing the melanophore pigmentation. 6 dpf larvae were used for all experimental procedures.

3. Antisense riboprobes synthesis and in situ hybridization (ISH)

Axon guidance antisense riboprobes were obtained from plasmids kindly provided by Prof. Driever (Universität Freiburg, Germany). Briefly, plasmids were linearized upstream of the target cDNA coding sequences while probes were transcribed from a downstream promoter. The transcription step was carried out in presence of digoxigenin-labelled nucleotides (SigmaAldrich, Italy), allowing the generation of tagged riboprobes against *slit 1a, slit 1b, slit 2, slit 3, netrin 1a, netrin 1b, robo3 var1, robo3 var2, dcc, robo 2* transcripts. In particular, purified plasmids for *netrin1a* and *dcc* were linearized with EcoRI and NotI restriction enzymes respectively. The digestion was carried out at 37°C for 4 hours. Once obtained the linearized plasmids, in vitro antisense riboprobes transcription was performed using T7 polymerase (2 hours at 37°C) (Promega, Italy). Transcribed antisense riboprobes were subjected to Turbo DNase for 1 hour incubation at 37°C and purified by "RNA Clean and Concentrator" kit (Zymo Research, Italy). Probes concentration was then measured by Nanodrop ND-1000 (ThermoFisher Scientific, Monza, Italy).

Larvae processed for ISH were fixed in 4% PFA and then subjected to methanol dehydration. The day of the experiment, samples were rehydrated stepwise, washed in PBT and permeabilized with Proteinase K (10 µg/ml, ThermoFisher, Italy) according to the stage. Samples were then post-fixed in 4% PFA and prehybridized in hybridization mix at 65°C. Subsequently, 200ng of antisense RNA probe were used for an overnight (O/N) incubation at 65°C. The following day, after several washes, larvae were incubated with anti-DIG antibody conjugated with alkaline phosphatase (SigmaAldrich, Italy) at 4°C O/N. Larvae were then extensively washed in PBT and then the alkaline phosphatase substrate NBT/BCIP (SigmaAldrich, Italy) was used to perform colorimetric detection. The staining was stopped with EDTA 1mM pH 5,5 in PBS and larvae were fixed in 4% PFA. Larvae were then mounted in 87% glycerol and acquired using Leica DMR microscope.

4. Protein extraction and western blot

Proteins were extracted from zebrafish dissected heads, dissected brains or primary cells. Samples were placed in Tissue Extraction Reagent (ThermoFisher, Italy) added with protease inhibitors (ThermoFisher, Italy) and phosphatase Inhibitors (ThermoFisher, Italy) to prevent protein degradation. Samples were next manually homogenized, subjected to sonication and then centrifuged at 13,000×g for 30 min at 4 °C. The supernatant was collected and protein concentration was determined by BCA Protein Assay Kit (ThermoFisher, Italy). Sample absorbance was measured at 540 nm by a spectrophotometric analysis. Concerning heparan sulfates epitope analysis, samples were extracted in 8 M urea, 50 mM Tris HCl pH 8 buffer, according to the protocol proposed by Nagase and colleagues (Nagase et al., 2021).

Extracted proteins were analysed by SDS PAGE. Protein lysates (10 µg) were supplemented with a 4x SDS sample buffer (ThermoFisher, Italy) containing 5% 2-Mercaptoethanol (SigmaAldrich, Italy), heated at 75°C for 10 min and run in precast acrylamide gels (4-12% Bis-Tris SDS-PAGE (ThermoFisher, Italy) in MOPS running buffer (ThermoFisher, Italy). Proteins were transferred on PVDF membranes (ThermoFisher, Italy) in 25 mM Tris, 192 mM glycine, 20% methanol (v/v) using the standard "sandwich" assembly and incubated with primary antibodies overnight at 4°C. Primary antibodies were used at 1:1000 final dilution. After washes in TBST, an incubation with secondary horseradish peroxidase (HRP)-conjugated antibody was performed at room temperature (RT) for 1 hour at 1:2000 final dilution. Primary and secondary antibodies used in western blot analysis are listed in *Tab1* and *Tab2*. Chemiluminescent signals were detected incubating the blotted membranes with the Supersignal West Pico Chemioluminescent substrate kit (ThermoFisher, Italy) and visualized by Image Quant Las 4000 (GE Healthcare, Italy) and analysed by ImageJ software (https://imagej.nih.gov/ij/). When needed, membranes were stripped using a commercially available solution (Restore PLUS Western blot stripping buffer (ThermoFisher, Italy).

5. Whole mount immunofluorescence on larvae and brains

Whole mount immunofluorescence was performed on 4% PFA fixed larvae or brains. Samples were incubated in Tris HCl 150 mM pH 9 for 5 min and then placed at 70°C for 15-20 min (brains/larvae respectively). Larvae were then washed in PBT (PBS+0,1% Tween-20, SigmaAldrich, Italy) while brains were rinsed in PBS Triton (PBS+TritonX-100 0,25% ThermoFisher, Italy). Saturation was performed with specific blocking buffers:

- Larvae: 1% BSA, 10% sheep serum, 0,8% Triton X-100 in PBT;
- Brains: 1% BSA, 2% sheep serum, 1% DMSO in PBS Triton 0,25%.

Primary and secondary antibodies were generally used at 1:100 final dilution (see *Tab3* and *Tab4*). One-day long incubations were applied to larvae while brains were incubated O/N. Labelled larvae and brains were then mounted on 1,5% low melting agarose for confocal imaging.

6. Zebrafish-derived primary neuronal cell cultures

Brains were dissected from 2 dpf bleached larvae as previously described (Patel et al., 2019). Brain pools were collected in HBSS supplied with penicillin/streptomycin (ThermoFisher, Italy) at RT. Cell dissociation was performed by 5 mg/ml Collagenase II (ThermoFisher, Italy) incubation for 20 min at 37°C. Isolated cells were centrifuged at 800 g for 5 min and the pellet was resuspended in culture medium. Complete medium was composed by DMEM/F-12, HEPES (ThermoFisher, Italy) supplemented with 2% penicillin/streptomycin-glutamine (ThermoFisher, Italy), 1% N2 supplement (ThermoFisher, Italy), 2% B-27 supplement (ThermoFisher, Italy), 0,25 µg/mL Amphotericin B (ThermoFisher, Italy), 0,1% BSA (SigmaAldrich, Italy), 2mM Glutamine (ThermoFisher, Italy) and 0,5 µg/mL Rifampicin (SigmaAldrich, Italy). Approximately 400.000 cells were seeded on poly-lysinated wells (SigmaAldrich, Italy) and maintained at 28°C. Cell medium was replaced after 1 day in vitro (DIV). Bright field images were taken using Leica DMIL LED microscope, 40x objective.

7. Immunofluorescence and lysotracker staining on primary cell culture

For immunofluorescence assays, primary cell cultures were fixed with 2% PFA supplied with 1 mM $CaCl_2$, 1 mM $MgCl_2$ and 4% sucrose for 10 min RT. After rinsing twice with PBS, blocking was performed with 10% sheep serum in PBS for 1 hour at RT. Primary antibodies were incubated O/N at 4°C. After two washes with PBS, cells were incubated with secondary antibody supplemented with 5,5 µM Hoescht (ThermoFisher, Italy) at RT for 1 hour and finally washed with PBS (see *Tab3* and *Tab4*).

For Lysotracker staining, primary cultures were incubated with Lysotracker Red 500nM (ThermoFisher, Italy) for 1 hour at 28°C, and post-fixed according to the abovementioned protocol. After one wash in PBS, cells were incubated with 0,1 mg/ml concanavalin (ThermoFisher, Italy) 5,5 µM Hoechst (ThermoFisher, Italy) for 10 minutes at RT to label whole cell membranes and nuclei, respectively. All samples were mounted with Fluoromount (ThermoFisher) and processed by confocal microscopy.

8. Microfluidic assays

Microfluidic chambers (Xona Microfluidics, XonaChip 150µm) were coated with poly-lysine (SigmaAldrich, Italy) according to manufacturer's guidelines. Approximately 200.000 cells were seeded on one side of the device; in this phase, 20 µl of cell medium (composition abovementioned) were added to the opposite chamber to restrain the cells inside the seeding compartment, thus preventing microgrooves crossing. A 20 µl volume difference was set between the seeded and empty chambers; since this difference could be maintained up to 24 hours, it needed to be re-established at 1 DIV by fresh medium addition. Cultures were then maintained at 28°C for 2 DIV. For cell membranes and nuclei visualization, cells were incubated with 0,1 mg/ml concanavalin (ThermoFisher, Italy) and 5,5 µM Hoechst (ThermoFisher, Italy) for 10 minutes, rinsed with PBS and acquired by confocal microscopy.

9. Confocal analysis

Whole larvae and whole brains were analysed by confocal microscopy using Nikon C2 H600L confocal microscope (Milan, Italy), 20x or 40x immersion objectives with Z-stack of approximately 3 µm. For 3D reconstructions, NIS-Elements Viewer (Nikon, Italy) software has been used.

Fluorescent images of primary cell culture and microfluidic device were acquired using Leica Stellaris confocal microscope equipped with a charge-coupled device camera and processed with the Leica LASX software. Each field was acquired with a Z-stack of 1 µm using a 63x immersion objective (cell culture immunofluorescence) or 0,5 µm and 40x immersion objective (microfluidic devices). For each coverslip at least six or seven fields were acquired. Confocal images were processed using ImageJ software (https://imagej.nih.gov): thresholded area and integrated density of the total sum of slices per field were used to compare the different genotypes. Pearson's coefficient was calculated using the JaCoP plugin for the colocalization between p62/Dcc.

10. Separation of subcellular fractions: fractional precipitation

Fractional precipitation was performed on 2 dpf head lysates: dissected heads were collected in in PBS supplemented with PMSF 1x and then manually homogenized (in a glass potter and with a glass pestel) in Tris 1 mM, EDTA 2 mM pH 7,4 buffer supplemented with protease and phosphatase inhibitors (ThermoFisher, Italy) (Julie A. Gosney, 2016 Thesis). Head extracts were subjected to a 3 min 800 g centrifugation and surnatants, at the final concentration of 1,5 mg/mL, were loaded on the top of a sucrose gradient (5% - 20% - 38% sucrose in Tris 1m M, EDTA 2 mM pH 7,4). Subsequent ultracentrifugation (Beckman Optima L-90K Ultracentrifuge) was performed with SW 60 Ti Swinging-Bucket Rotor (Beckman Coulter, Italy) at 40.000 rpm for 1 hour at 4°C, slow acceleration and no brake. Fractions were recovered manually from the top to the bottom of the column according to the volumes of each sucrose fraction, and then concentrated exploiting the trichloroacetic acid (TCA) - Na-deoxycholate (DOC) method and speed vacuum (Savant SVC 100H Speed Vac Concentrator). Pellets were

resuspended in 1x SDS sample buffer (ThermoFisher, Italy) and analysed by western blot as previously described.

11. Retinotopic mapping

For retinotopic mapping, 6 dpf Ath5 GCaMP:GFP wt and *ids* mutant larvae were placed in a 2% low melting agarose drop and analysed by two-photon microscopy with a 16x objective (Bergamo I Series, Thorlabs, Newton, NJ, United States). Larvae were placed at 90°C with respect to a 3 cm far display on which stimuli were projected. In particular both looming and moving stimuli, generated in Python using Stytra (Štih et al., 2019) were presented monocularly. Controlateral retinal ganglion cells tectal projections were recorded by whole brain scanning (volume covered 100 × 100 × 55 μm^3) and analysed through a custom Python script.

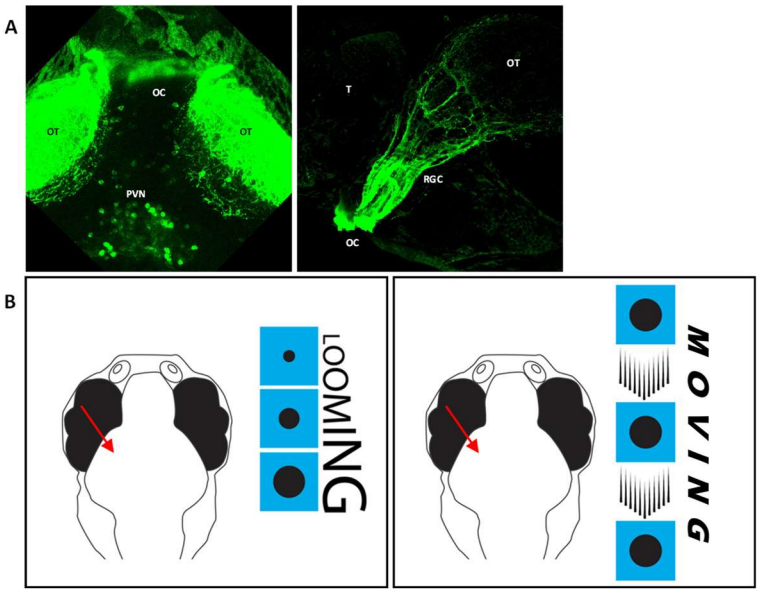

Retinotopic mapping. (A) *Representative confocal Z-stack projections of the brain derived from a 6 dpf Ath5 GCaMP:GFP reporter larva.* ***(A, left)*** *The image focuses on the midbrain region; the fluorescent signal can be traced at the level of the optic tectum and periventricular neurons. Dorsal view with anterior to the top.* ***(A, right)*** *The image depicts the fluorescent signal detected at the level of the retinal ganglion cell projections towards the optic tectum. Lateral view with anterior to the left.* ***(B)*** *Schematic representation of the two trials (looming and moving dots) used during 2-photon whole brain recordings. The red arrow points to the region in which fluorescent signal was recorded (optic tectum contralateral to the stimulated eye). OT: optic tectum; PVN: periventricular neurons; OC: optic chiasm; RGC: retinal ganglion cell arborization; T: telencephalon.*

Basically, each pixel track was compared with the stimulation track in time; this led to the definition of *coefficients* and *scores*.

The *coefficient* indicated was correlated to pixels intensity for a given stimulation (higher coefficients corresponded to higher response intensity), while with *scores* we referred to pixels responses variability (higher scores corresponded to higher reliability in the analysis).

12. Behavioural assays

12.1 Prey-capture assay

Wild type and *ids* mutant larvae were challenged with paramecia at 6 dpf. The behavioural set up was composed by an arena, a watch glass in which the larvae could freely move, and a camera (Ximea) placed above. The haunting test lasted one hour; the number of paramecia was counted at the beginning and at the end of the test by a 10 s recording.

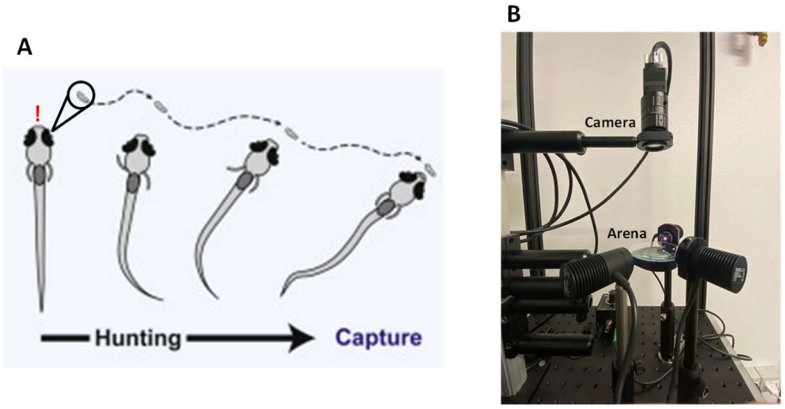

Prey-capture assay. (A) *Schematic representation of the hunting and capture behavior of a zebrafish larva stimulated with paramecia (adapted from Henriques et al., 2019).* ***(B)*** *Image of the behavioral set up used for the prey-capture assay. The arena in which larvae were stimulated consisted of a watch glass placed under a recording camera.*

12.2 Random dot motion test

Free swimming larvae were tested with the random dot motion test projected underneath (stimuli were generated in Python using Stytra). The test was composed by 10 s intervals in which dots moved randomly alternated to 10 s intervals with dots moving with a given coherence, referred as the proportion between “directioned” and “random” moving dots (0,3 – 0,6 – 1%). Dots directions were adjusted with respect to the fish position inside the arena. Larval movements were recorded and tracks analysis was performed through a custom Python script.

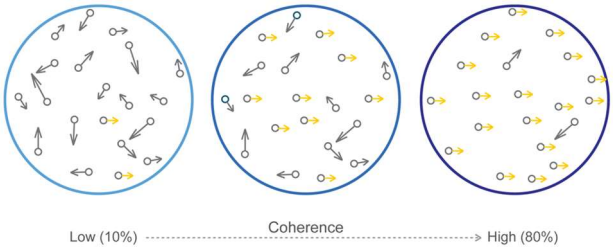

Random dot motion test. *The image visually represents the coherence level of a random dot motion test. Dots directions are depicted by arrows. Moving from the left to the right panel, a higher number of dots are moving in the same direction (higher coherence), as shown by yellow arrows (Robertson et al., 2012).*

12.3 Anxiety-like test

6 dpf larvae were placed in a multi-well and tested with Danio vision (Noldus, Netherlands). The trial consisted of 10 min of light alternated with 10 min of complete darkness, repeated four times. Noldus software allowed to track movements and obtain larval position in time. Centroid analysis was then performed through a custom Python script. Larvae were genotyped after phenol-chloroform DNA extraction and PCR using primers for *ids* gene (for 5'-TGTGTTCTTTCAAAGCAAG; rev 5'-TTGTGGTGTCTGGTCTTCGA). PCR products were visualized in 3% agarose gel (Low EEO, ThermoFisher, Italy).

13. Statistical analysis

Results were expressed as mean ± SD (standard deviation). Data were analysed using two-tailed unpaired/paired Student's t test for comparison between two groups. p values <0.05 were considered statistically significant. The confidence level for significance was 95%. Data were analysed using Prism software version 8 XLM (GraphPad Software).

Tab1. Western Blot Primary antibody

Epitope	Code	Host
Netrin1	LSBio, LS-B5912	Goat
Dcc	Antibodies Online, ABIN2782671	Rabbit
pFAK (Tyr397)	ThermoFisher, 44-624G	Rabbit
FAK (C-20)	Santa Cruz, sc-558	Rabbit
N-WASP	Novus, NBP1-82512	Rabbit
GFAP	Abcam, ab154474	Mouse
CDH2	Genetex, GTX125885	Rabbit
LAMP1	Developmental Studies Hybridoma Bank, 1D4B	Rabbit
P62	Cell Signaling, #5114	Rabbit
Rab7	Abcam, ab50533	Mouse
LC3B	SigmaAldrich, L7543	Rabbit
HS (10E4)	US Biological, H1890	Mouse
β-actin	Santa Cruz, sc-56459	Mouse
GAPDH	Abcam, ab9485	Rabbit

Tab2. Western blot secondary antibody (HRP-conjugated)

Name	Code
Anti- Mouse	Bethyl, A90-116P
Anti-Rabbit	Jackson ImmunoResearch, 111-035-019
Anti-Goat	SigmaAldrich, A8919

Tab3. Immunofluorescence primary antibody

Epitope	Code	Host	Dilution
Dcc	Antibodies Online, ABIN2782671	Rabbit	1:150
HS (10E4)	US Biological, H1890	Mouse	1:50
Acetylated tubulin	SigmaAldrich, T7451	Mouse	1:100
GFAP	Abcam, ab154474	Mouse	1:100
P62	Progen, GP62-C	Guinea Pig	1:200

Tab4. Immunofluorescence secondary antibody (fluorophore-conjugated)

Name	Code	Dilution
Anti-Mouse FITC	ThermoFisher, F2761	1:100
Anti-Rabbit TRITC	ThermoFisher, A16101	1:100
Anti-Guinea Pig FITC	Jackson ImmunoResearch, 106-095-003	1:200

RESULTS

1. netrin1a and *dcc* display altered expression pattern in *ids* mutant larvae

Early mechanisms of MPS II CNS-related pathogenesis are far to be completely understood. Nevertheless, a previous transcriptomic analysis on the brain of the MPS II mouse model revealed that, among a plethora of signaling and metabolic pathways-related transcripts, axon guidance (AG) molecules appeared severely dysregulated (Salvalaio et al., 2017). By the fact that no data are reported for the zebrafish counterpart and given *ids* essential function during embryonic development (Moro et al., 2010), I focused my attention on the analysis of AG-molecules in the *ids*-mutant zebrafish larvae.

To this purpose, I started my investigation by performing an *in situ* hybridization-based screening. Indeed, thanks to the collaboration with Professor Driever (University of Freiburg, Germany), I collected a set of plasmids containing the coding sequence of some AG-related molecules (*netrin1a, netrin1b, dcc, slit1a, slit1b, slit2, slit3, robo2, robo3*) from which I derived the corresponding antisense riboprobes. All probes were then tested on mutant and control zebrafish larvae at 24 and 48 hpf (*data not shown*). Among these markers, *netrin1a* and *dcc* expression patterns appeared the most dysregulated ones in the head of *ids* mutant larvae with respect to controls. Interestingly, Netrin/Dcc axis represents one of the main pathways involved in chemoattraction during axon guidance. In particular, at 24 hpf *netrin1a*-positive signal was traceable in the ventral optical area, in the ventral region of midbrain and hindbrain, with a higher concentration at the midbrain-hindbrain boundary. This pattern was maintained both in control and mutant larvae, with controls showing higher overall signal intensity (*Fig.1A upper panels*). Similarly to *netrin*, also *dcc* appeared dysregulated in the head of mutant larvae at the same time point: in wild type (wt) fish, *dcc*-positive areas were mostly found in the ventral midline of the hindbrain, while in mutants this signal was almost completely missing (*Fig.1A lower panels*). At 48 hpf, *netrin1a* signal was still present at the optic disk and the ventral midline but with higher

intensity and wider rostro-caudal extension in *ids* mutant larvae when compared to age matched controls. In both genotypes, a positive staining was also evident at the margins of the optic tectum (*Fig.1B upper panels*). Concerning *dcc*, the signal concentrated in the rostro-ventral region of the hindbrain in mutant fish with respect to controls (*Fig.1B lower panels*). Considering that the most evident differences between wt and mutant were related to *dcc* and *netrin*, I decided to select them for further analyses.

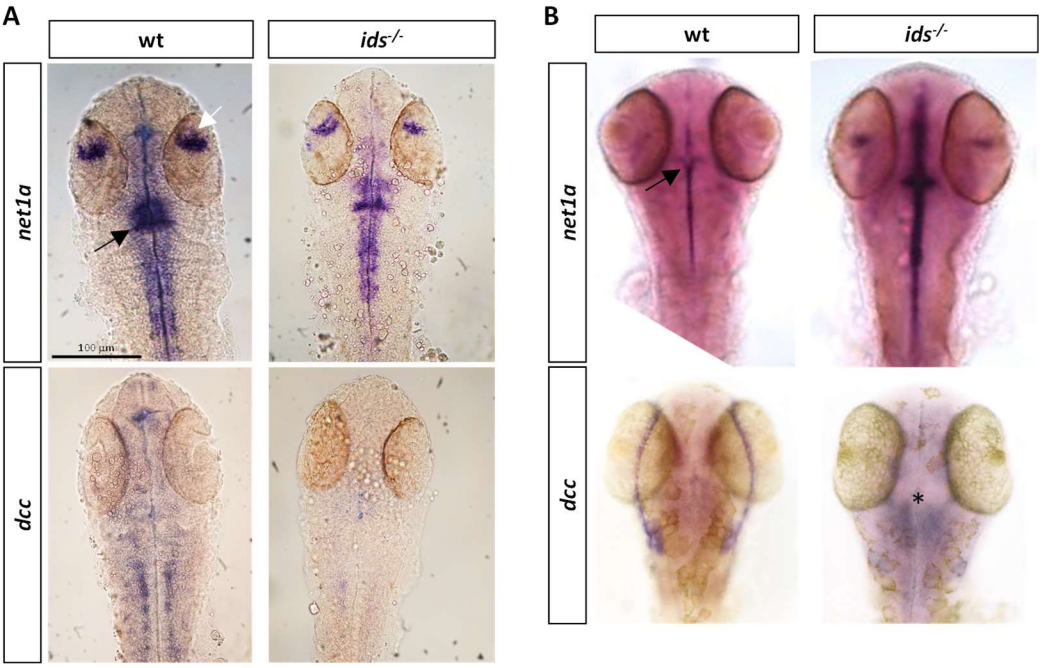

Fig. 1. netrin 1a and dcc expression is dysregulated in ids mutant larvae. (A) *Representative in situ hybridization at 24 hpf. The upper panels show representative netrin1a in situ hybridization on ids mutant and age matched controls. A positive signal is traceable in the medial region and at the midbrain-hindbrain boundary (black arrow). A white arrow points netrin1a positive staining in the eye region. Overall, mutant larvae report a reduced signal intensity compared to controls. The lower panels depict dcc in situ hybridization in wt and ids mutant larvae. In controls, dcc signal concentrates around the medial region of the hindbrain while in mutants is barely traceable.* ***(B)*** *Representative in situ hybridization at 48 hpf. netrin 1a in situ hybridization on wt and ids larvae (upper panels). The medial signal is maintained in both genotypes with mutants displaying higher intensity. Netrin1a ocular staining is clearly traceable in the eye of mutants and less evident in controls. The black arrow indicates the midbrain-hindbrain boundary. Lower panels report representative dcc in situ hybridization. An asterisk (*) points dcc-enriched hindbrain region in mutants. Tectal staining visible in controls is almost missing in mutant larvae. All images are dorsal views with anterior to the top.*

2. Dcc, but not Netrin1, protein levels are dysregulated in *ids* mutant derived heads

Once depicted the expression patterns in mutant and control larvae, I proceeded with Netrin1 and Dcc quantitative evaluation. A time course protein analysis on wild type head extracts revealed that the temporal window of Netrin1 expression was extremely precise and restrained between 2 and 5 days post fertilization (dpf); before and after this interval, Netrin was undetectable by western blot (*Fig. 2A*). For this reason, when looking at Netrin1 protein levels, I mainly focused on 2 and 3 dpf as time points. By comparing controls and mutants Netrin1 relative amount, I could not find any significant difference (*Fig. 2B-C*). On the other hand, Dcc levels were significantly higher in mutant lysates with respect to control ones already at 24 hpf (*Fig. 2D*). The same difference of Dcc protein levels was consistently found also at 48 hpf (*Fig. 2E*). In addition, to spatially localize Dcc-positive (Dcc+) domains, I performed whole mount immunofluorescence on control and *ids* mutant larvae. At 24 hpf (*Fig. 2F upper panels*), Dcc was clearly expressed by cells of the developing pineal gland, placed rostrally to the posterior commissure between the forebrain and midbrain. The pineal gland was found positive for Dcc staining also at 2 dpf (*Fig. 2 F lower panels*); at this stage, and only in mutant *ids* larvae, Dcc signal was traceable at the level of the intertectal commissures primordia, a series of big axonal fascicles involved in interhemispheric communication. Therefore Dcc, but not its ligand Netrin, showed a significant dysregulation not only in mRNA but also in protein level in mutant fish. For this reason, I decided to focus my efforts on the study of Dcc transmembrane receptor and its modulation during control and mutant zebrafish brain development.

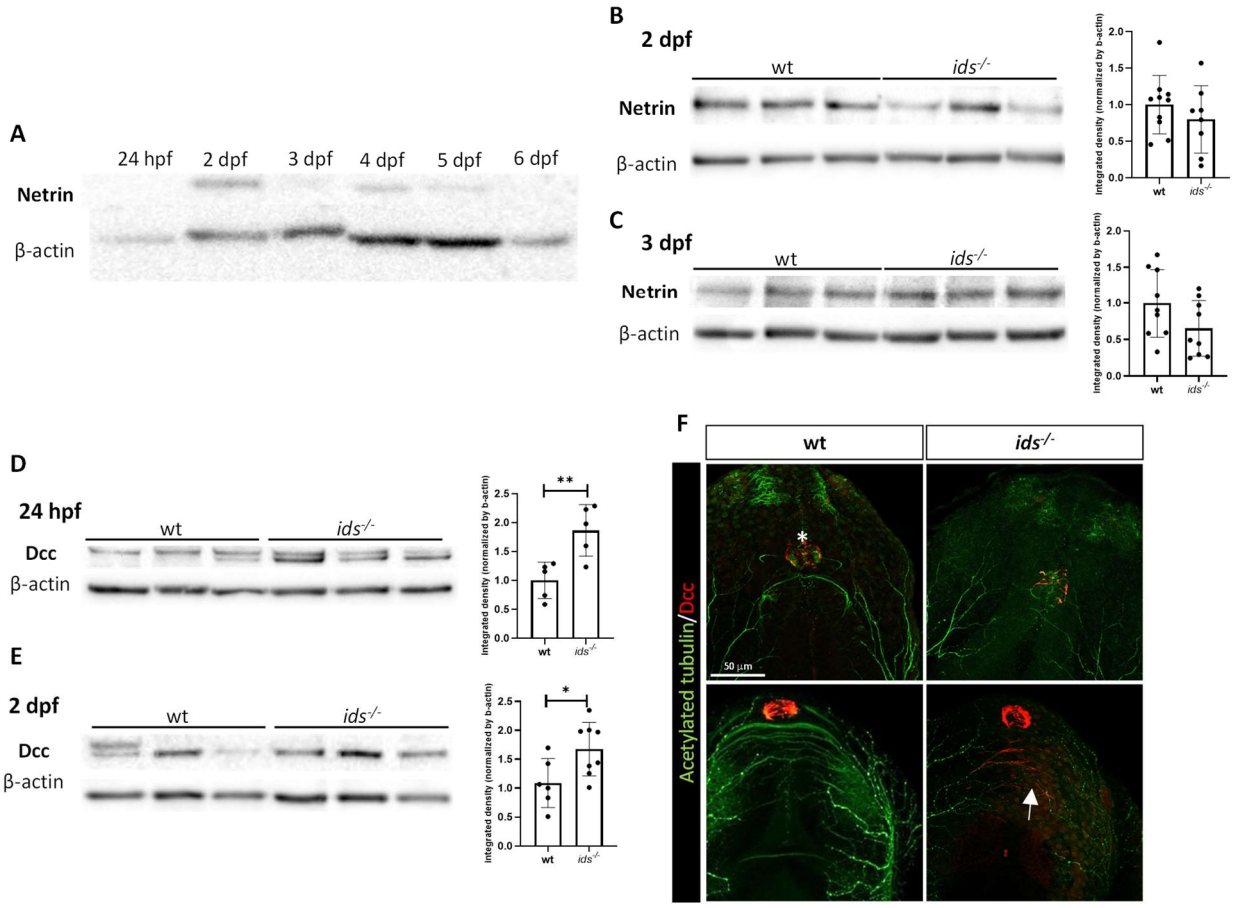

Fig. 2. Dcc protein levels are dysregulated in ids mutant heads. (A) *Western blot analysis of Netrin1 on wild type head protein lysates at different time points: the band is traceable between 2 and 5 dpf. Western blots on 2 dpf* ***(B)*** *and 3 dpf* ***(C)*** *head protein extracts reveal no significant differences between ids mutants and age matched controls. Dcc protein levels are significantly upregulated both at 24 hpf* ***(D)*** *and 2 dpf* ***(E)*** *in the head of mutant larvae with respect to age matched controls. For western blot analysis, at least five biological replicates (pools of 20 dissected heads) were tested for each genotype.* ***(F)*** *Representative whole mount immunofluorescence for acetylated tubulin (green) and Dcc (red) (dorsal view with anterior to the top). At 24 hpf (upper panels) Dcc is expressed at the level of the pineal gland (*) in both genotypes. At 2 dpf (lower panels), ids mutant larvae show Dcc-positive signal at the intertectal commissures (white arrow); this staining is almost completely missing in control larvae (n=10). Data are expressed as the mean ± SD (* p<0.05; **p<0.005; t-test).*

3. Dcc is upregulated in the brain tissue of MPS II larvae

Although Dcc protein levels were consistently higher in *ids* mutants, whole head analysis could be affected by the concomitant presence of different tissues including, cartilages and eyes, which can express Dcc (Bosserhoff et al., 2014; Vigouroux et al., 2020). To assess whether the quantitative difference of Dcc protein levels detected in *ids* mutants could be related to the brain component, I established a robust protocol for larval brain dissection starting from 2 dpf larvae. In agreement with the results obtained on whole heads, Dcc upregulation was consistently detectable by western blot on mutant-derived brain lysates at 48 hpf, as well as at 3 dpf and 6 dpf (*Fig. 3A*). These data confirmed Dcc misexpression in the brain of MPS II fish. In addition, I performed whole mount immunofluorescence on dissected brains from control and MPS II larvae at 6 dpf (*Fig. 3B*): a positive Dcc staining was traceable around blood vessels, pineal gland region and intertectal fascicles, as already pointed out at 2 dpf in the whole larva. Interestingly, by looking at midbrain commissures by confocal 3D reconstructions I found that, while in control fish Dcc was localized on the entire axonal tract, commissures in mutant fish brains were Dcc-positive only in the lateral and not in the medial region. The ratio between the number of the axon displaying Dcc immunoreactivity in the entire length and the total Dcc-positive commissures was significantly different between mutant and control brains.

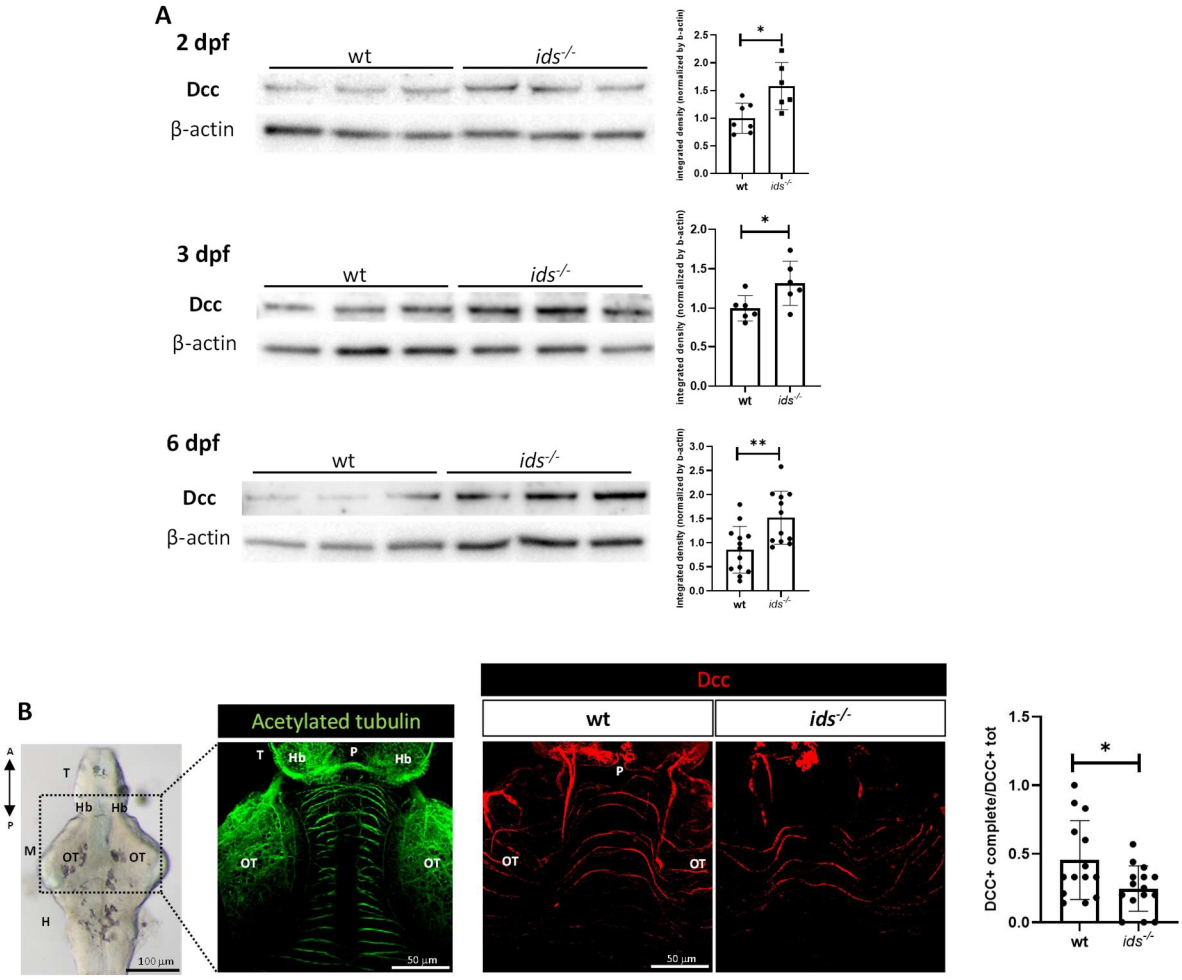

Fig. 3. Dcc protein levels are dysregulated in ids mutant brains. (A) *Western blot analysis on brain derived-protein extracts at 2, 3 and 6 dpf revealed significantly upregulated Dcc levels in mutants when compared to controls. At least six biological replicates (pools of 20 dissected brains) were tested for each genotype.* ***(B, left)*** *Immunofluorescence analysis of Dcc localization focused on the midbrain region highlighted both in the bright field and in a representative whole mount brain immunofluorescence for Acetylated tubulin; dorsal view with anterior to the top.* ***(B, right)*** *Representative dcc whole mount brain immunofluorescence on 6 dpf wild type and ids mutants (imaging depth ~200 µm). The bar graph shows the ratio between the number of the axon displaying Dcc immunoreactivity in the entire length (Dcc+ complete) and the total Dcc-positive commissures (Dcc+ tot) for each genotype (n=14/15 brains). Data are expressed as the mean ± SD (* p<0.05; **p<0.005; t-test). T: telencephalon; Hb: habenula; OT; optic tectum; M: midbrain; H: hindbrain; P: pineal gland.*

4. Isolated brains showed alterations in Dcc downstream targets

To evaluate whether higher Dcc levels were paralleled by an increased activation of the downstream pathway, I analysed pFak and N-Wasp relative abundance by western blot analysis. Indeed, Fak autophosphorylation at Tyr-397 is one of the first events following receptor activation, leading to a downstream complex intracellular cascade which culminates in cytoskeletal rearrangements orchestrated by N-Wasp activity and the mediation of actin-dependent motile processes (Shekarabi et al., 2005).

At 2 and 3 dpf, *ids* mutant-derived brains exhibited no difference, when compared to controls, in pFak/Fak ratio, despite significantly higher levels of both forms. On the other hand, no variations between genotypes were evident for N-Wasp. When moving to 6 dpf, I found that while activated (pFak) and total Fak amounts showed no differences between mutants and control brain-derived protein extracts, N-Wasp was significantly downregulated in *ids* mutant brains (*Fig. 4*).

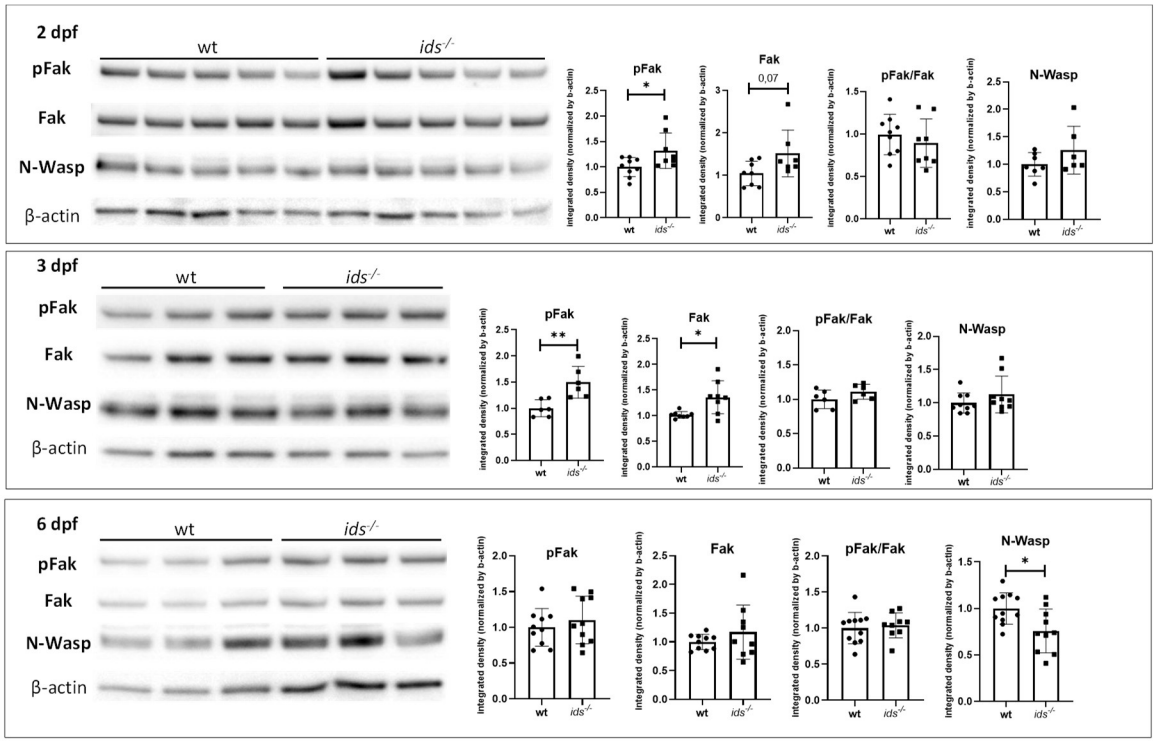

Fig. 4. Western blot analysis of Netrin/Dcc downstream effectors. *Western blots showing no significant variations between mutants and controls neither in pFak-Fak ratio nor in N-Wasp protein levels in 2, 3 and 6 dpf brain extracts. pFak and Fak are significantly upregulated in mutant-derived brain extract at 2 and 3 dpf when compared to controls. At least five biological replicates (pools of 20 dissected brains) were tested for each genotype. Data are expressed as the mean ± SD (* p<0.05; **p<0.005; t-test).*

5. Dcc upregulation involves the neuronal compartment of the brain

Analysis of whole brain showed consistent Dcc upregulation in mutant fish, but the brain is a heterogeneous tissue composed by different cell types such as neurons, radial glia and endothelial cells. To find out whether receptor dysregulation was affecting the neuronal population, I scaled up the resolution of my investigation with the establishment of an optimized protocol for zebrafish-derived neuronal cell cultures. In the setup phase, I started from manually dissected brain pools at 2 dpf and tested different cell dilutions and culture media. Moreover trypsin, EGTA/EDTA, collagenases have been tested as dissociation methods to evaluate their impact on Dcc epitope preservation (*data not shown*). I initially took advantage of an available transgenic zebrafish line *Tg(neuroD:GFP)* (Casari et al., 2014), to easily identify neurons by looking at GFP signal (*data not shown*). Once plated, dissociated brain cells start to adhere and develop first processes after a few hours; at 2 days *in vitro* (DIV) isolated neuronal cells have already formed an intricate connection network (*Fig. 5A*). Cell cultures can be maintained up to 4 DIV prior to cell death. Since axonal growth takes place very quickly *in vitro*, the model becomes extremely suitable for axonal development-related studies. Furthermore, to assess the magnitude of "contamination" by non-neuronal cell types (glial cells) that may express axon guidance molecules, I tested Glial Fibrillary Acidic Protein (Gfap) protein levels on primary neuronal cell cultures both by western blot and immunofluorescence. In fact, it is known that also astroglial cells participates in the guidance process by shaping the extracellular environment around the axons (Barresi et al., 2005). While at 1 DIV Gfap protein levels were barely detectable (very low intensity compared to total brain lysate), at 2 DIV they were no longer traceable by western blot, suggesting that the culture conditions were responsible for a progressive glial cell deprivation, leading to a consequent neuronal enrichment (*Fig. 5B*). This was confirmed by immunofluorescence on 2 DIV cells which showed a high number of Acetylated tubulin-positive cells (*Fig. 5C*) and very low percentage of Gfap-positive cells (about 6%) (*Fig. 5D*).

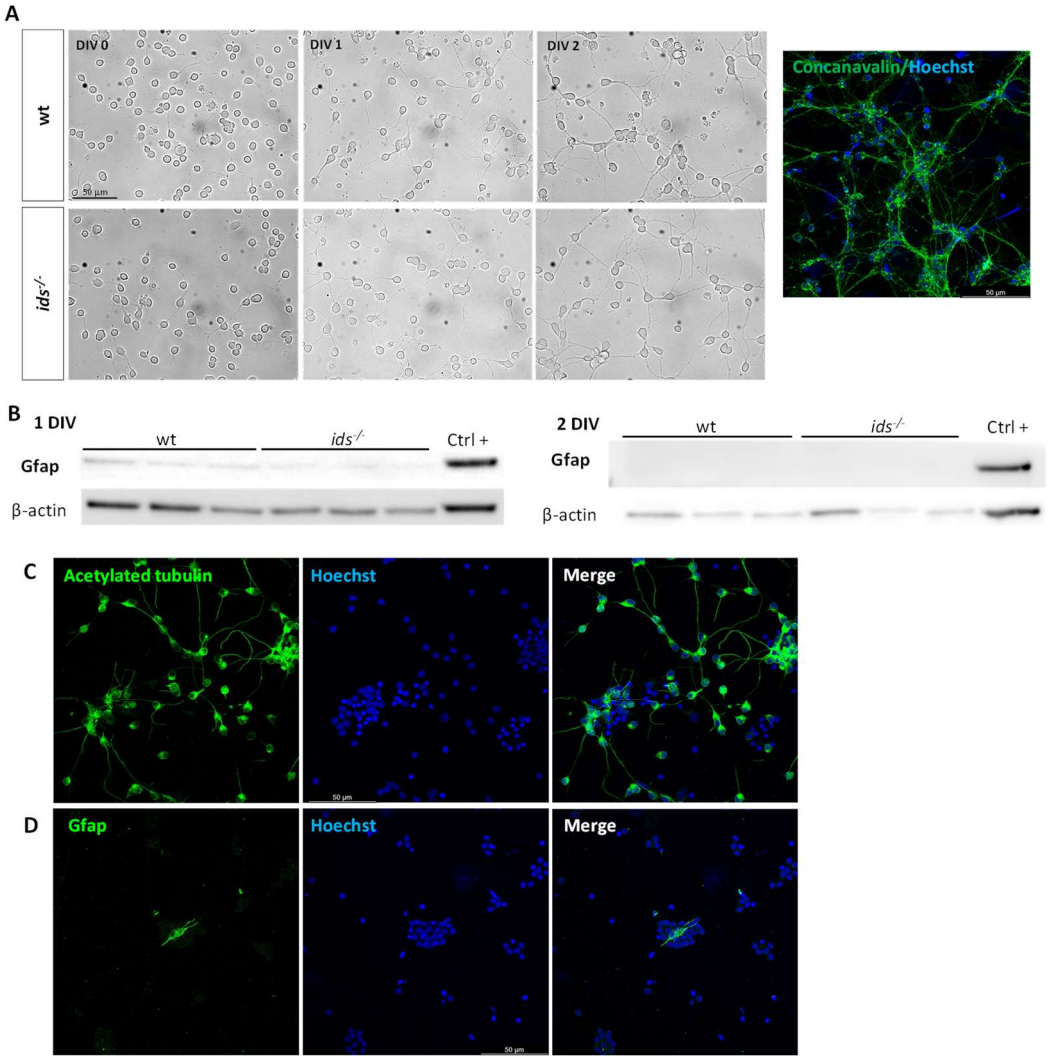

Fig. 5. Characterization of zebrafish primary cell culture. (A) *Bright field images of wild type and mutant-derived primary cell cultures from 0 to 2 days in vitro. On the right, a representative confocal image of a 2 DIV culture stained with Hoechst (nuclei, blue) and concanavalin (membranes, green) is reported.* ***(B)*** *Western blot analysis of Gfap levels of wild type and mutant-derived cell culture protein extracts compared to a positive control (whole brain extract). The analysis was conducted both at 1 DIV (left) and 2 DIV (right).* ***(C)*** *Representative Acetylated Tubulin/Hoechst immunofluorescence on wild type-derived cell culture at 2 DIV.* ***(D)*** *Representative Gfap/Hoechst immunofluorescence on wild type-derived cell culture at 2 DIV. As evident from the image, the percentage of Gfap-positive cells is very low when compared to total nuclei number.*

By exploiting this newly established cellular model, I tested both Dcc and its downstream molecular targets. At 6 hours *in vitro* (HIV), when first processes become evident and axons start their growth, no differences have been measured in Dcc or pFak/Fak ratio whereas N-Wasp showed significantly higher levels in mutant-derived cells when compared to controls (*Fig. 6A*). Dcc upregulation became evident at 2 DIV in mutant-derived neurons, confirming the dysregulation seen in total heads and dissected brains. Moreover, Dcc immunostaining showed that mutant-derived primary neurons presented an increased number of Dcc-positive dots when compared to the control condition (*Fig. 6B-C*). In the same protein lysates derived from mutant neuronal cells both phosphorylated FAK, but not total Fak and N-Wasp, showed increased protein levels with respect to controls (*Fig. 6B*).

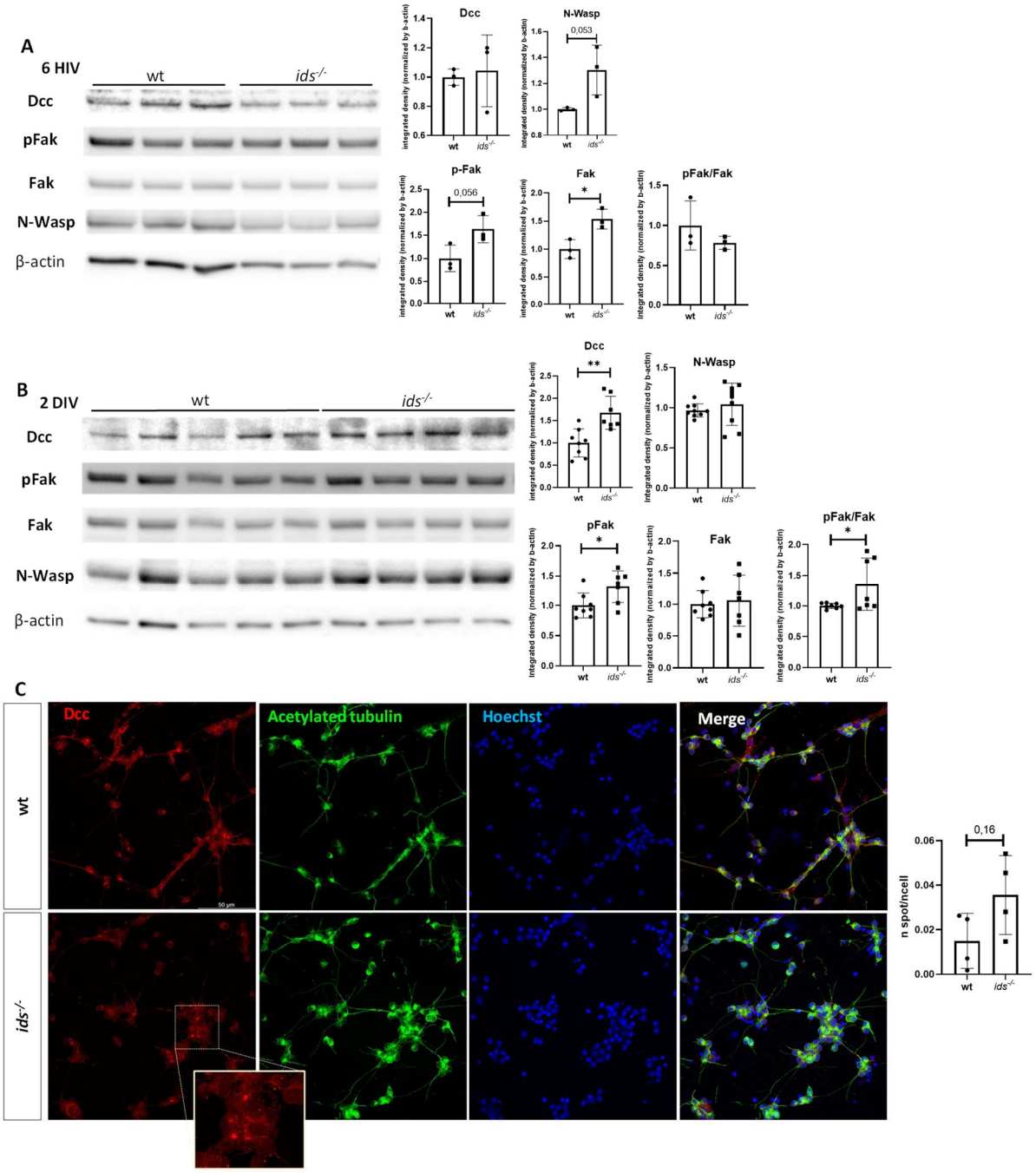

Fig. 6. Analysis of Dcc and its downstream target in neuronal primary cultures. (A) *Western blot analysis on 6 HIV mutant and control-derived primary cultures (n=3, obtained by 24 dissected brains each).* ***(B)*** *Western blot analysis on 2 DIV mutant and control-derived primary neuronal cultures (n=7 biological replicates, obtained by 24 dissected brains each). At this time point, Dcc and pFak are significantly upregulated in mutant-derived cell cultures.* ***(C)*** *Representative immunofluorescence for Dcc (red) and Acetylated Tubulin (green) on primary neuronal cultures at 2 DIV. Dcc spots are depicted the magnification are. The bar graph on the right shows the number or Dcc-positive spots normalized on the total cell number. Data are expressed as the mean ± SD (* p<0.05; **p<0.005; t-test).*

6. Dcc protein is detected in p62-enriched cytosolic fraction mutant larvae

Receptors are not fixed on the plasma membrane but they are involved in a dynamic shuffling between cell surface and intracellular space. Indeed, upon ligand binding, they are rapidly endocytosed to be stored and recycled or degraded through the endolysosomal pathway (Konopacki et al., 2016). It has been reported that defective lysosomal function can have a deleterious impact on vesicles trafficking. Furthermore, alterations of vesicle homeostasis have been found as a key factor in the MPS IIIA neuro-pathology (Fecarotta et al., 2020; Keating et al., 2012). In light of these premises, I explored Dcc intracellular localization in MPS II zebrafish larvae.

To this purpose I set up a novel original protocol for fractional precipitation of zebrafish heads lysates at 2 dpf. By optimizing the procedure proposed by Gosney (Julie A. Gosney, 2016 Thesis), I was able to retrieve membrane (N-cadherin-positive), cytosolic (Glyceraldehyde-3-Phosphate Dehydrogenase, Gapdh-positive) and vesicles (Rab7-positive) enriched fractions by a sucrose gradient (*Fig. 7A*). Once assessed the reproducibility of the protocol, both wt and *ids* mutant head lysates were parallelly loaded on the top of the sucrose gradient and subjected to ultracentrifugation for fractionation. For both genotypes I was able to obtain a good and reproducible separation. When checking Dcc distribution, I found that it mostly localised in the low-density sucrose fractions (*Fig. 7B*). Concerning fractional precipitation of wt head lysate, Dcc was mainly co-sedimenting with lipidated microtubule-associated protein 1A/1B-light chain 3 (LC3II), together with Rab7 and Lamp1. On the other hand, Dcc-enriched fractions of mutant-derived lysate fractionation contained, in addition to LC3II, higher levels of the ubiquitin-binding adaptor protein p62 (also known as Sqstm1 or p62) and very low amount of Rab7/Lamp1 (Lysosomal-associated membrane protein 1) (*Fig. 7C*). Moreover, this result was paralleled by the evaluation of Dcc-p62 co-localization by immunostaining and Pearson's coefficient analysis: even if not significant, mutant-derived primary neurons at 2 DIV exhibited a higher Pearson's coefficient when compared to controls, confirming a higher Dcc-p62 association (*Fig. 7D*).

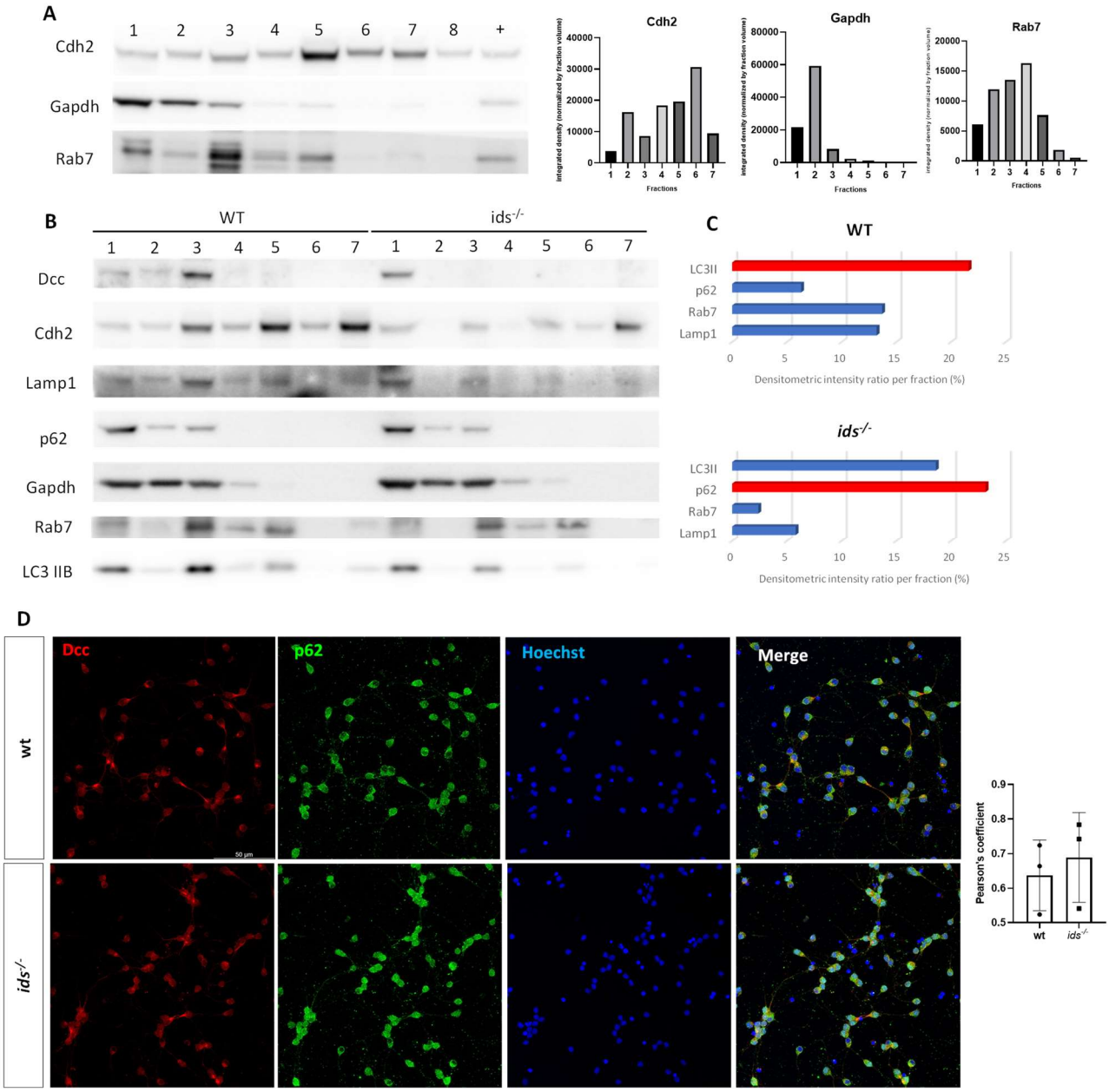

Fig. 7. Analysis of Dcc localization. (A) *Western blot showing successful fractionation of wild type-derived head protein lysate. Cdh2 (plasma membrane), Gapdh (cystosol) and Rab7 (late endosomes) proteins are enriched in different fractions. Fractions were collected from the top (1) to the bottom (8) of the column. A total head lysate was used as positive control. The bar graphs on the right show Cdh2, Gapdh and Rab7 distribution inside the different fractions; fraction 8 is not reported because was enriched in cell debris. Integrated densities were normalized on fractions volumes.* ***(B)*** *Representative western blot of wild type and mutant-derived protein extract subjected to ultracentrifugation.* ***(C)*** *The bar graphs report the main proteins present in Dcc-enriched fractions. For controls, fraction 3 composition is shown; for ids mutants, the graph depicts fraction 1 (the only one containing Dcc). The x axis represents the densitometric intensity of marker normalized on the total densitometric intensity of the analyzed fraction (percentage). A red filled bar is in correspondence of the most abundant protein of the fraction.* ***(D)*** *Representative immunofluorescence for Dcc (red) and p62 (green) on 2 DIV primary cell cultures (n=3). The graph reports the results of Dcc-p62 colocalization analysis (Pearson's coefficient). Data are expressed as the mean ± SD of three independent assays (t-test).*

To explore whether increased Dcc-p62 colocalization could be ascribed to impaired lysosomal function, I carried out Lysotracker staining on wt- and mutant-derived primary neuronal cell cultures. At 2 DIV, mutant-derived neurons showed significantly decreased Lysotracker-positive lysosomes when compared to controls (*Fig. 8A*). This result was supported by western blot analysis at the same time point, showing significantly higher Rab7 protein levels in mutant-derived neuronal cell extracts when compared to those of control cells (*Fig. 8B*).

Therefore, from this set of analysis I could conclude that, in *ids* mutant conditions, Dcc preferentially localized with p62/LC3B-II rather than Rab7/Lamp1. Moreover, mutant brain-derived cells showed a decrease in lysotracker staining when compared to controls.

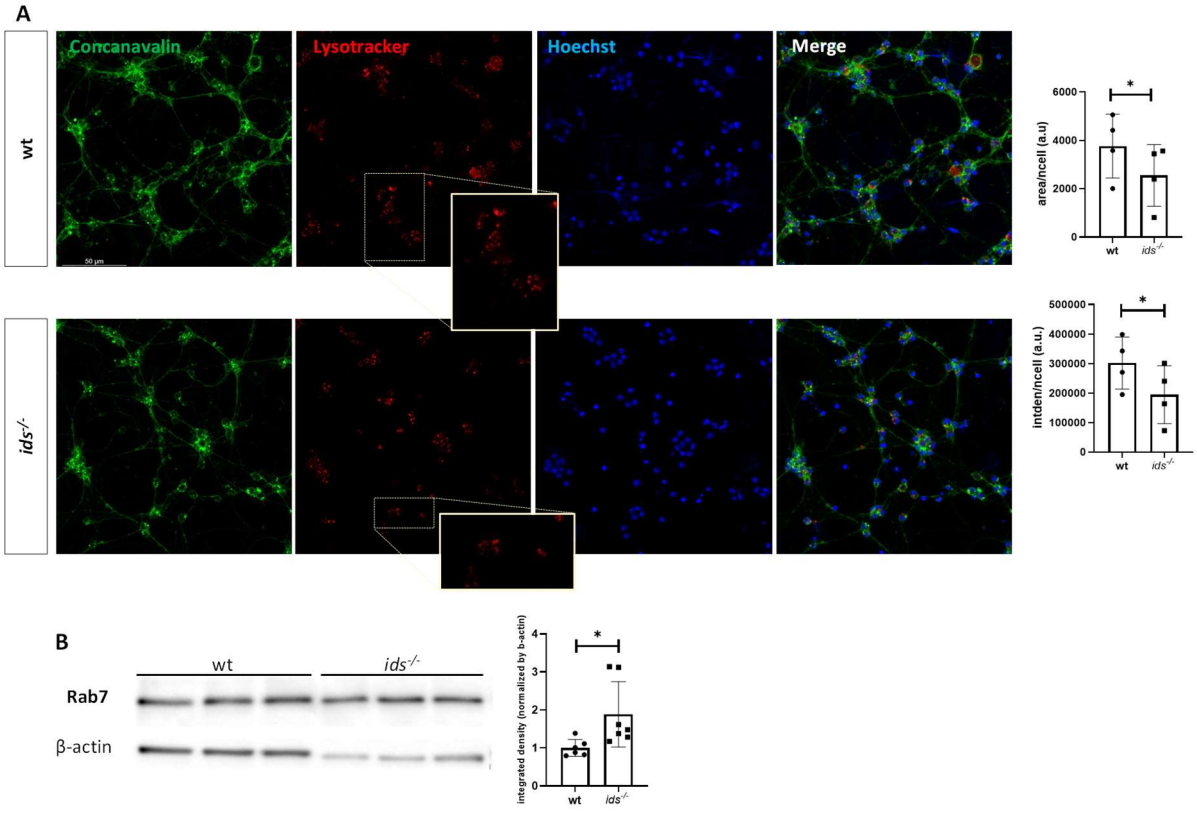

Fig. 8. ids mutant-derived primary cell cultures display altered lysotracker staining and Rab7 protein levels. (A) *Lysotracker staining (red) on wild type and ids mutant-derived primary cell cultures at 2 DIV. Concanavalin (green) and Hoechst staining (blue) are reported to visualize cell membranes and nuclei, respectively. Magnifications of Lysotracker staining highlight reduced signal in mutant-derived cells. On the right, bar graphs show the area and integrated density quantification. In both cases, mutants show a significant decrease when compared to controls (n=4).* ***(B)*** *Western blot analysis of Rab7 protein levels: 2 DIV mutant-derived cell cultures show significant upregulation of Rab7 with respect to controls. Data are expressed as the mean ± SD of at least 6 biological replicates, obtained by 24 dissected brains each (* p<0.05; t-test).*

7. Mutant-derived neurons project shorter axons

To assess whether MPS II neurons may exhibit characteristic phenotypic abnormalities and to better understand the dynamics of their axonal elongation, I decided to apply the newly established primary neuronal cell cultures to a dedicated commercial microfluidic device. This tool consists of two or more chambers communicating through channels that selectively allow only axonal crossing, creating a physical separation between cell somas and processes. Thanks to these microfluidic devices, it became simple to follow axonal growth and assess axonal length (*Fig. 9A*). These tools are also designed to create a volume-dependent diffusion gradient of specific molecules that can be applied on one chamber: in this case, the applied molecules can flow and reach the target axons, according to a volume-dependent flow. After adapting the protocol to primary zebrafish cells, I was able to seed both control and *ids* mutant neuronal cells and maintain them in culture for 2 days. To investigate their phenotype at basal conditions, I first evaluated axonal extension without any stimulation and by only applying different volumes to the chambers; this created a constant flux from the soma region to unseeded compartment. By confocal analysis, I observed that both control and mutant neurons can extend axons through the microchannels, with mutant cells showing more branched axons. In addition, when measuring axonal length from the soma, I consistently found that mutant-derived neurons exhibit significantly shorter axons when compared to the control ones (*Fig. 9B*).

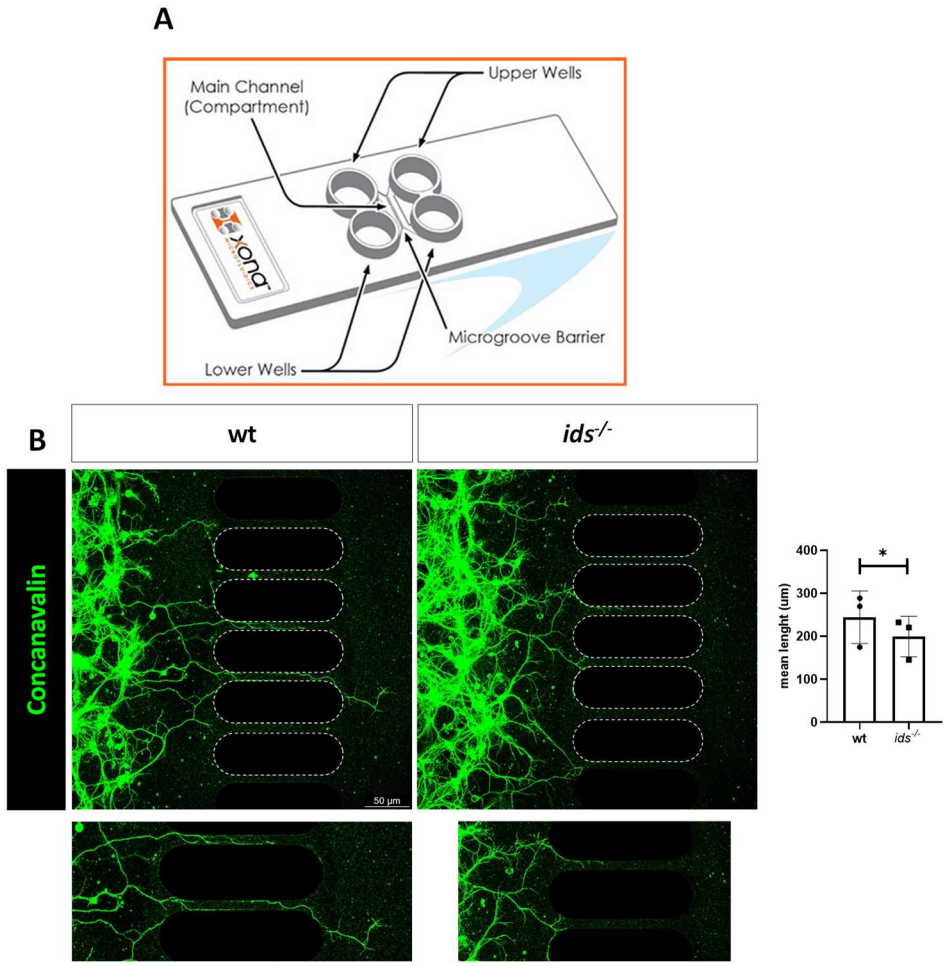

Fig. 9. ids mutant-derived primary neurons show shorter axons when compared to controls. ***(A)*** *Scheme of the microfluidic device that has been exploited (XonaMicrofluidics). It is constituted by four wells and two main compartments divided by a microgroove barrier. Cells are seeded in one chamber and axons extend in the other one.* ***(B)*** *Representative confocal images of wild type and ids mutant derived primary neurons seeded in the microfluidic device (2 DIV). Cultures were stained with concanavalin to easily trace processes. Below, magnifications of crossing axons. The graph at the right resumes the results obtained by measuring crossing-axons lengths (n=3). Ids-derived neurons presented consistently shorter axons when compared to controls at 2 DIV. Data are expressed as the mean ± SD (* p<0.05; t-test).*

8. Undetectable gross heparan sulfate changes but evident mislocalization at the choroid plexus of *ids* mutant larvae

Heparan sulfates (HS) can bind both ligands and receptors to modulate signaling cascades (Smock and Meijers, 2018). Indeed, since both Netrin and Dcc have been proven to interact with HS and HS accumulation has been considered a hallmark of Mucopolysaccharidosis, I preliminary analysed HS relative abundance by western blot. When comparing wild type and mutant total head lysates, no significant differences were reported neither at 2 dpf nor at 3 dpf (*Fig. 10A*). When looking at HS by immunofluorescence, I detected a widely spread signal in the brain region from 2 to 5 dpf, with a positive signal close to blood vessels (*data not shown*). Since this signal became more precise around the pineal gland, I decided to concentrate my attention on this telencephalic region. By looking at whole brain immunofluorescence at 6 dpf, I was also able to identify a HS-positive structure placed rostrally to the pineal gland: this was identified as the choroid plexus, one of the major components of blood cerebrospinal fluid barrier. Interestingly, this structure showed a very different architecture when comparing wild type and *ids* mutant brains, in which it appeared more disorganized (*Fig. 10B*).

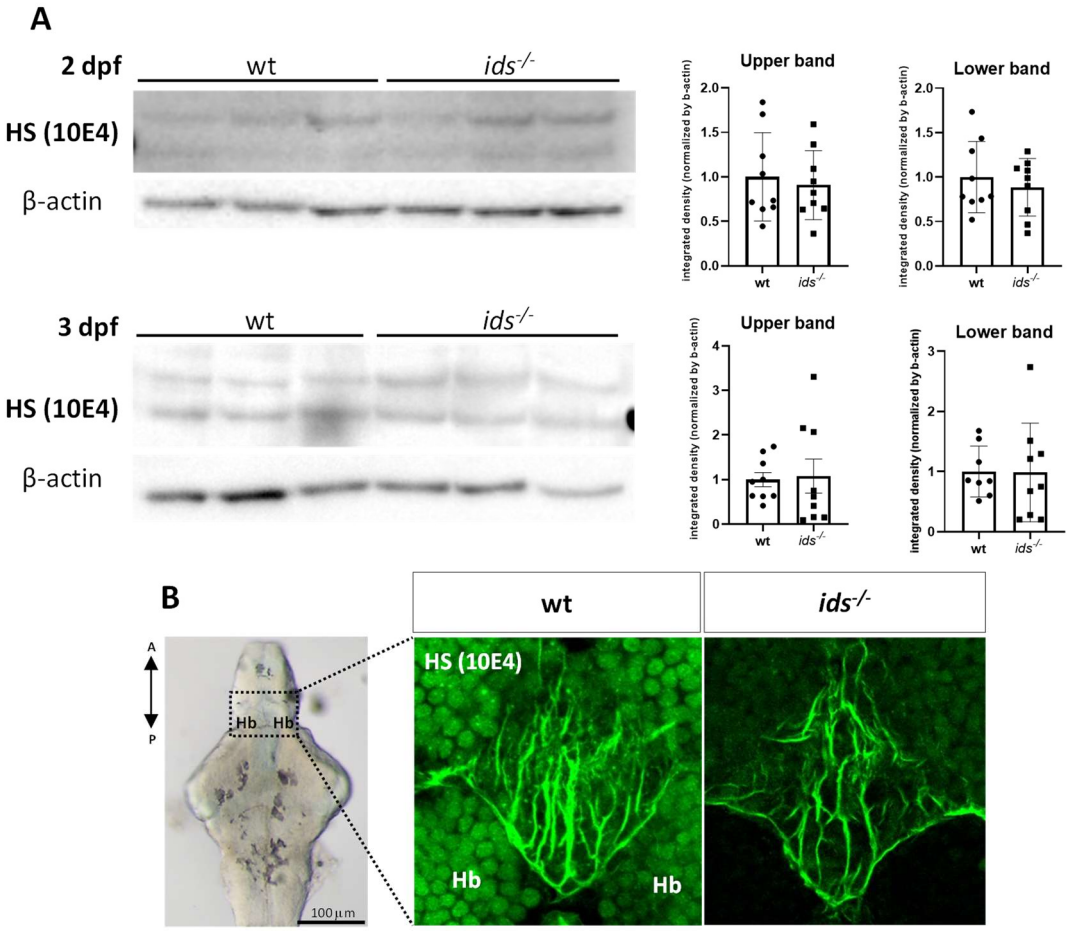

Fig. 10. ids mutant larvae did not show alterations in total HS levels. (A) *Heparan sulfate (10E4) analysis by western blot at 2 and 3 dpf. Ids-derived head protein extracts did not show significant differences when compared to controls (n=9, pools of 20 dissected heads).* ***(B)*** *Whole mount HS (green) immunofluorescence on 6 dpf extracted brains. The bright field image on the left depicts the localization of the analyzed structure (dorsal view with anterior to the top). On the right, confocal images magnifications of wild type and ids mutant choroid plexus are reported. Ids-derived brains display altered choroid plexus morphology (n=10). Data are expressed as the mean ± SD (t-test). Hb: habenula.*

9. Higher Dcc levels are still traceable at mature stages in *ids* mutant brain

Dcc/Netrin axis is crucial not only during development, but it is also involved in synapse maintenance and homeostasis in the adult brain (Vosberg et al., 2020). To find out whether Dcc upregulation in *ids* mutants was restricted to the developmental phase or it was maintained even at later stages, I performed western blot on isolated brain lysates from 3 months old and 2 years old wt and mutant fish. In these adult stages, brain protein samples could be separated in different anatomical compartments such as forebrain, midbrain and hindbrain, thus allowing a more precise indication of Dcc distribution with respect to the whole brain analysis. At 3 months, when fish reach their sexual maturation and adulthood begins, Dcc levels were significantly higher in mutant-derived hindbrain when compared to the control condition (*Fig. 11A*). This upregulation was still visible at 2 years, the most mature stage of zebrafish life. At this time point, Dcc was upregulated also in the forebrain and midbrain regions (*Fig. 11B*). Therefore, the hindbrain-restricted upregulation seen at 3 months in mutant brains became generalized to the whole brain by 2 years.

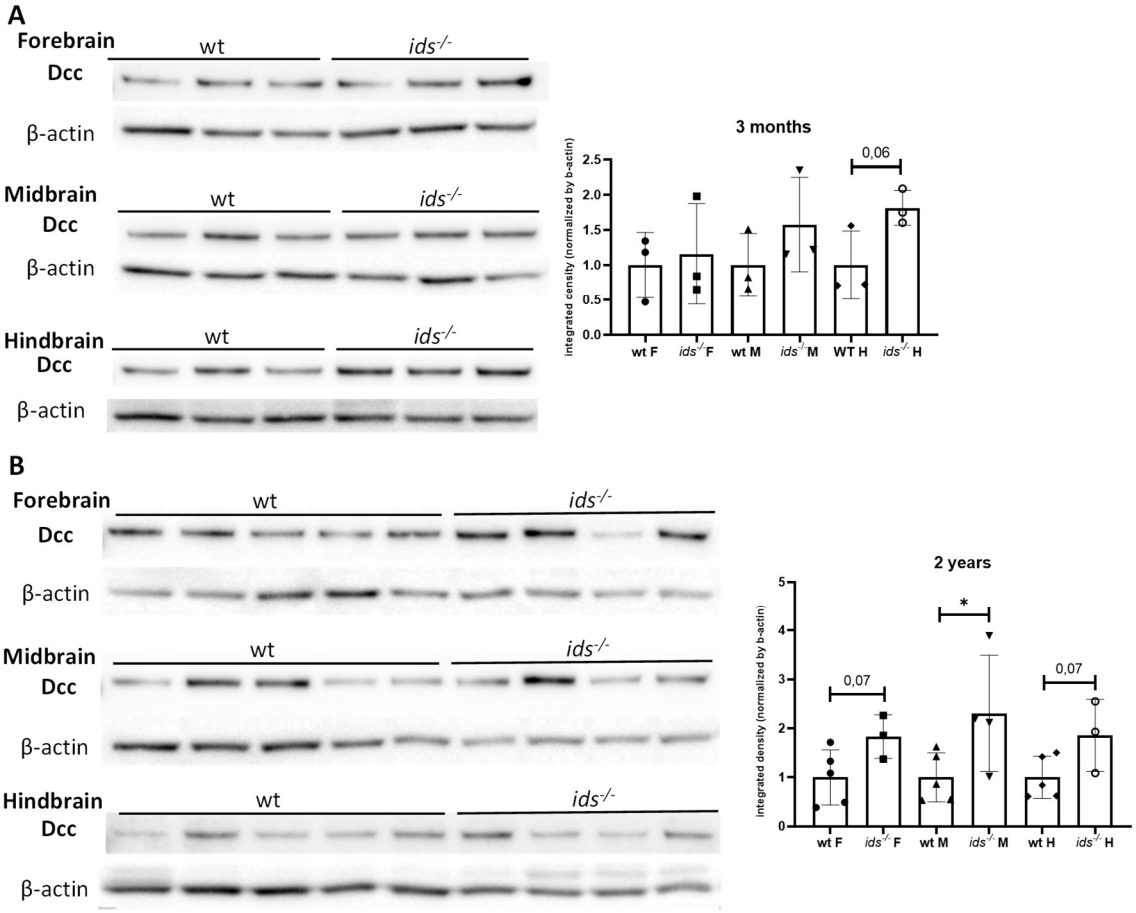

Fig. 11. Dcc protein levels are dysregulated at in the MPS II adult fish. (A) *Representative western blot showing Dcc epitope detection in wild type and ids-derived brains at 3 months; forebrain, midbrain and hindbrain regions were tested independently (n=3, pools of 6 brains). Mutant fish derived brain samples showed nearly significant Dcc upregulation, when compared to controls, in the hindbrain region.* ***(B)*** *Representative western blot for Dcc in wild type and ids-derived brains at 2 years; forebrain, midbrain and hindbrain regions were tested independently (at least 3 biological replicates). In mutant derived brains, Dcc upregulation was significantly higher in all regions. Data are expressed as the mean ± SD (* p<0.05; t-test). F: forebrain; M: midbrain; H: hindbrain.*

10. *ids* mutant-derived brain show dysregulated Gfap levels by juvenile phase

During axon guidance, glial cells play a fundamental role in shaping the extracellular environment creating precise paths axons can follow (Rigby et al., 2020). Moreover, astrocytes activation and neuroinflammation are listed among the major cellular pathological events and clinical symptoms of neuronopathic MPS II, recapitulated by the 6 weeks old murine disease model (Zalfa et al., 2016). However, no data regarding these mechanisms have been reported for the MPS II zebrafish model. To this purpose, I carried out a western blot-based time course analysis of Gfap protein levels from embryonic (2 dpf) to adult (2 years) stages. Indeed, Gfap is a universally recognized marker for activated astrocytes: it is a structural protein involved in the maintenance of astrocytes and BBB architecture; while in physiological conditions its levels are kept extremely low, increased Gfap levels are usually associated with pathological changes and neuroinflammation. This is due to astrocytes proliferation and hypertrophy: astrocytes that undergo this kind of activation are usually referred as "reactive" (Wilhelmsson et al., 2006). In 2 and 6 dpf whole brain extracts, no differences between controls and *ids* mutants have been detected in Gfap levels (*Fig. 12A-B*). In these embryonic stages Gfap-positive cells differentiate and play a supportive role for the developing brain. Starting from 1 month of age, instead, forebrain, midbrain and hindbrain regions were isolated from mutant and control fish. At 1 month, the stage which marks the beginning of the juvenile period, midbrains derived from *ids* mutant fish showed significantly increased Gfap levels with respect to controls; in forebrain and hindbrain structures Gfap abundance was comparable between the genotypes (*Fig. 12C*). The same midbrain-related Gfap upregulation was consistently found also at 3 months old, when fish become adults and reach sexual maturity (*Fig. 12D*). Finally, I analysed Gfap levels in 2 years old wild type and *ids* mutant-derived brains. This represents the most mature stage of zebrafish life, comparable to the elderly phase of human beings. At this time point, significantly higher Gfap levels were scattered throughout the entire brain of mutants when compared to controls (*Fig. 12E*).

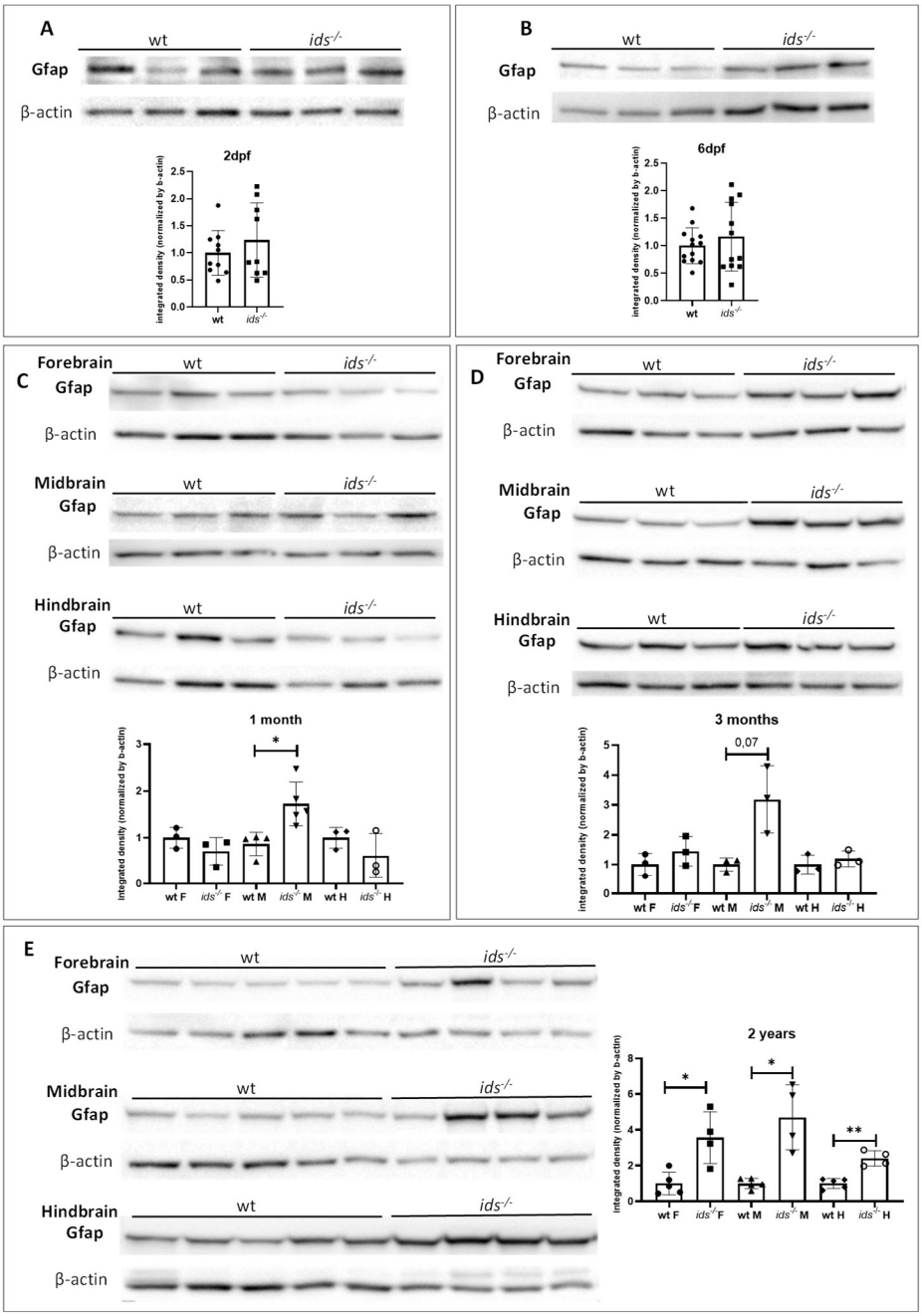

Fig. 12. Time course analysis of Gfap protein levels reveals dysregulation since juvenile stages in ids mutant brains. *Representative Gfap western blot at 2 dpf* ***(A)*** *and 6 dpf* ***(B)*** *show no significant differences between ids and control fish-derived brains (at least 9 biological replicates, pools of 20 dissected brains each).* ***(C)*** *Representative western blot for Gfap in 1 month old ids mutant and controls brains; forebrain, midbrain and hindbrain regions were tested (at least 3 biological replicates, pools of 6 dissected brains each). Mutant dish derived brain lysates showed significant Gfap upregulation, when compared to controls, in the midbrain region. The same upregulation was consistently found in western blot analysis at 3 months* ***(D)****; forebrain, midbrain and hindbrain regions are tested independently (at least 3 biological replicates, pools of 6 dissected brains each).* ***(E)*** *Representative western blot for Gfap analysis in wild type and ids-derived brains at 2 years; forebrain, midbrain and hindbrain regions were tested independently (at least 4 biological replicates). In mutant derived brains, Gfap upregulation was spread to the entire brain. Data are expressed as the mean ± SD (* p<0.05; t-test). F: forebrain; M: midbrain; H: hindbrain.*

11. A preliminary phenotypic characterization of mutant larvae revealed subtle but not significant behavioural defects

The visual system is one of the most accessible and easily recognizable CNS structure in which axon guidance and HS are involved. Indeed, Netrin/Dcc pathway has been recognized as fundamental for correct optic nerve fasciculation at the optic stalk (Deiner et al., 1997). Once crossed the midline at the optic chiasm, AG-molecules guide the optic nerve towards the optic tectum where it arborizes in different layers. When studying the visual system in the zebrafish model, it is possible to analyse both the arborization and the visual-induced behaviours thanks to specific reporter lines and behavioural set ups, respectively (Bollmann, 2019). Therefore, since MPS II patients show visual-related symptoms such as retinal degeneration and impaired stimuli integration, we asked whether these phenotypes could be recapitulated in a MPS II zebrafish model which showed defects in Dcc levels and localization.

To this purpose, I firstly took advantage of the Ath5 GCaMP:GFP transgenic zebrafish line with the aim of describing retinotopic maps. Ath5, also known as atoh7 or atonal bHLH transcription factor 7, is a transcription factor involved in retinal ganglion cells (RGCs) genesis and maturation. In the transgenic line, these cells express a recombinant form of Calmodulin linked to the GFP protein. In resting condition, Calmodulin hides GFP resulting in minimal fluorescence intensity; instead, when calcium is released from intracellular storages in response to neuronal excitation, Calmodulin-calcium binding exposes GFP with consequent peaks of fluorescence. Therefore, whole brain recordings were taken on wild type and *ids* mutant Ath5 GCaMP:GFP zebrafish larvae at 6 dpf: two photon microscopy analysis allowed to trace neuronal activation in response to looming and moving visual stimuli. No significant differences were evident between the two genotypes, neither in retinotopic mapping (obtained by analysing the position flaring regions triggered by specific visual stimuli inside the optic tectum) (*Fig. 13A*) nor in GFP signal intensity (*Fig. 13B*). Nevertheless, control larvae showed higher variability when compared to mutant ones.

I next performed a prey-capture test using paramecia to analyse whether visual stimuli could be integrated in a coherent behaviour (hunting). In agreement with confocal brain recordings, 6 dpf control larvae showed a more variable phenotype with respect to control but, overall, no differences were seen in hunting performance (*Fig. 13C*). Finally, free swimming larvae were tested in an open field arena: moving dots were presented underneath and larval movements were recorded. Among these dots, some of them moved randomly while others moved in the same direction. In this set up, the coherence level is defined as the proportion between the number of "directioned" and "random" moving dots: at higher coherence levels correspond low difficulty of the task (Robertson et al., 2012). When analysing zebrafish motions, high coherence levels are usually paralleled by high number of "correct movements", referred as swimming arrangements towards the direction of the moving dots (Harpaz et al., 2021). Even if not significantly different, while control larvae showed a trend of increased correct movements correlating with increased dots coherence, *ids* mutants response remained the same regardless of the coherence (*Fig. 13D*).

Finally, I performed the well-established "light-dark challenge" test to evaluate anxiety-like responses (Rock et al., 2022). Indeed, anxiety is one of the main manifestations affecting MPS II patients. In this behavioural set up, 6 dpf larvae subjected to light/dark alternation and movement were recorded. No differences were reported between wild type and mutant larvae in total run distance. Moreover, we performed centroid analysis which consist in the evaluation of the position occupied by the fish inside the well during light and darkness frames. Due to high heterogeneous responses, controls and mutant patterns were not significantly different. However we could conclude that, in both genotypes, darkness phase triggered exploration of the central region, whereas during light fish preferred to move along the borders of the wells (*Fig. 13E*). Therefore, no striking differences neither in visual nor anxiety-related behaviours could be identified at larval stages.

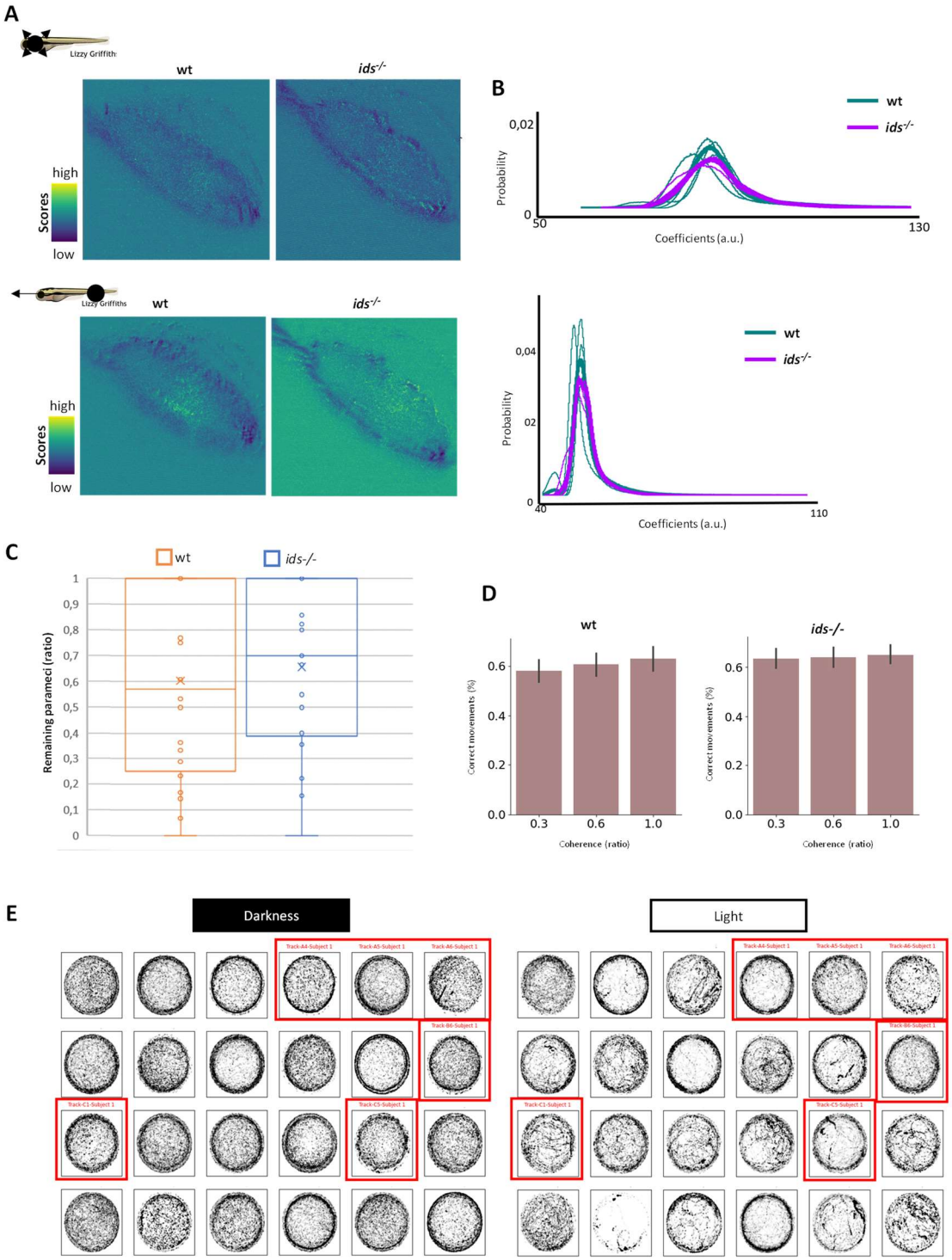

Fig. 13. Retinotopic mapping and behavioral test did not show significant differences between wild type and ids mutant larvae. (A) *Reconstruction of retinotopic mapping of Ath5 GCaMP:GFP zebrafish larvae at 6 dpf subjected to visual stimulation. The type of stimulation (looming or moving dot) is reported in the scheme on the left. Regions with higher scores are depicted in yellow while low scores pixels are shown as blue.* ***(B)*** *Graphical representation of coefficient related to looming and moving dot-induced responses. Each thin curve represents one single fish while bold ones represent the medium response. The curves graphically describe the distribution of arbitrary intensity values (coefficient) in the retinotopic map of wt and mutant larvae subjected to visual stimulation. ids mutant and wild type curves almost coincide (at least n=3 different subjects).*

(C) *Graphical representation of hunting rate of 6 dpf wt and ids mutants challenged with paramecia. On the y axis, the ratio between the number of remaining paramecia at the end of the trial and the number of paramecia present at the beginning of the test is reported (n=12 different subjects).* ***(D)*** *The graph shows the percentage of "correct" movements associated with moving dots with different coherence levels (n=8 different subjects).* ***(E)*** *Centroid analysis of 6 dpf zebrafish larvae subjected with dark and light alternation. Each square contains the movement of a single larva inside a well. The right picture depicts larvae movements in complete darkness while the scheme on the left illustrates the motions of the same fish during light intervals. Darker zones are the ones most frequently covered by larvae motions. Red frames highlight mutant larvae tracks, un-framed tracks are the ones of control larvae (n=12 controls; n=6 ids mutant larvae; larvae were genotyped a posteriori).*

DISCUSSION

Mucopolysaccharidosis type II (MPS II) is a rare X-linked syndrome belonging to the family of lysosomal storage disorders (LSDs). As the name LSD suggests, MPS II aetiology has been traditionally associated with the accumulation of undegraded glycosaminoglycans inside the lysosome, leading to organelle engorgement and dysfunction. Indeed, MPS II patients harbour mutations in the iduronate-2-sulfatase (*IDS*) gene which encodes a lysosomal hydrolase involved in the degradation of heparan (HS) and dermatan sulfate (DS), resulting in decreased or absent catabolic activity. These molecular perturbations translate into a plethora of symptoms, both somatic and neurological. In the most severe cases, in which the central nervous system (CNS) is involved, patients can show a critical neurodevelopmental delay from early childhood, seizure-like episodes and cognitive impairment that progressively worsens and becomes life-threatening (Barone et al., 2018). While somatic manifestations can be alleviated by enzyme replacement therapy, CNS-related symptomatology remains still untratable.

Since the late '90s, the mouse model has been exploited to unravel molecular mechanisms of MPS II CNS-related symptoms: neuroinflammation and astrogliosis seen from 6 weeks of age evolve into neurodegeneration and neuronal death by 1 year. More recently, also a stable MPS II zebrafish line has been generated and characterized at a somatic level, while its CNS-related pathology has still to be addressed. Interestingly, a bulk RNA sequencing performed on brains of 9 month old MPS II mice showed significant alterations in calcium signaling, synapse communication and axon guidance pathways (Salvalaio et al., 2017). In relation to the term *axon guidance,* we refer to all processes that allow the nascent axon to reach its target tissue. At the axonal tip, the growth cone orchestrates and integrates different stimuli deriving from the extracellular matrix, resulting in a highly dynamic structure. Both secreted and membrane-bound chemotactic molecules are implied in the establishment of very precise axonal routes. In this context, axons are supported by glial cells which function is to shape the

environment surrounding the axon to sustain correct pathfinding. Heparan sulfates play a key role during axon elongation: they modulate intracellular pathways by interacting with ligand-receptor complexes and restrict cues diffusion along the surface of receiving cells, preventing their dispersion in the extracellular space or aberrant signaling to other layers of cells (De Pasquale and Pavone, 2019). In fact, alterations of heparan sulfates homeostasis can negatively affect axon guidance and synapse formation (Lee and Chien, 2004).

Therefore, given AG-pathways dysregulation in the MPS II mouse brain and considering that *ids* downregulation has been reported to negatively affect early developmental processes in the zebrafish embryo, this thesis mainly focused on the investigation of AG-related molecules in the early stages of development of a MPS II zebrafish model.

An *in situ*-based screening identified *netrin1a* and *dcc* expression patterns as dysregulated in *ids* mutant larvae when compared to controls. These two molecules represent one of the most important axes involved in axonal chemoattraction and therefore play an essential role in CNS development (Boyer and Gupton, 2018). Netrin1a mRNA patterning resembled the one published by Lauderdale and colleagues in 1997 (Lauderdale et al., 1997): in this study the Authors suggested that glial cells, rather than neurons, were the ones responsible for *netrin1a* signal at the midline. Indeed, while this cell type locates in the medial region of the developing brain, neuronal cell bodies distribute laterally. In accordance with this hypothesis, glial cells are known regulators of axon guidance given their role in the secretion of AG-related cues (Ellezam et al., 2001; Rigby et al., 2020). Interestingly, by looking at *dcc* localization, it appeared clearly distributed in regions surrounding this medial region where glial cells are located. Therefore, this *dcc* signal symmetrically distributed around the midline could be mainly attributed to the neuronal cell type.

Since the differences detected by *in situ hybridization*, I started to investigate Netrin and Dcc at the protein level. Most studies concerning zebrafish Netrin1 refer only to mRNA levels and are restricted to the first stages of embryonic development (from 10 to 33 hpf) (https://zfin.org/). One manuscript analysed

Netrin1 expression at later time points (5 dpf) but it was mainly focused on the spinal cord (Rosenberg et al., 2014). No data are currently available concerning Netrin1 protein levels in the developing zebrafish. In this context, a time course analysis on dissected heads revealed that Netrin1 was detectable between 2 and 5 dpf, the temporal window in which the main CNS rearrangements take place (Boulanger-Weill and Sumbre, 2019). While Dcc was significantly upregulated since 24 hpf in mutant larvae heads, no differences between *ids* mutants and control were found for Netrin1. In agreement with these observations, Dcc dysregulation was consistently found in dissected mutant-derived brains also at 2, 3 and 6 dpf, directly confirming brain involvement. Furthermore, Dcc showed a differential patterning in wild type and mutant-derived midbrains at 6 dpf. In this region, intertectal commissures (ITC) were positively marked with mutants exhibiting lower percentage of commissure stained in their entire path. These commissural axonal fascicles derive from GABAergic interneurons of which somas reside in the mesencephalic tegmentum, placed rostrally to the midbrain–hindbrain boundary. ITC are involved in interhemispheric communication and are found essential in the binocular localization of the prey (Förster et al., 2020; Gebhardt et al., 2019). However, Dcc mislocalization was not sufficient to negatively impact on prey recognition in *ids* mutant larvae. This could be justified if considering that defective binocular integration transduced in a significantly impaired hunting efficiency only in an ITC-ablated condition (Gebhardt et al., 2019).

Moreover, I could demonstrate that Dcc upregulation was directly involving neurons by setting up an optimized and reproducible protocol for neuronal-enriched primary culture from 2 dpf dissected brains. Indeed, given the heterogeneity in tissue composition (i.e. endothelial cells, glia and neurons), total brain analysis was not sufficient to dissect which cell type/types is/are involved in Dcc upregulation. Several studies reported protocols for neural primary zebrafish cell cultures isolated from whole embryo (Acosta et al., 2018), spinal cord (Meade et al., 2019), adult brain (Russo et al., 2018) and embryonic brain (Patel et al., 2019; Chen et al., 2013). In particular, Patel and colleagues described how to

dissect 2 dpf zebrafish brain and maintain primary neural cells in culture up to 9 DIV. However, the addition of fetal bovine serum (FBS) and epidermal growth factor (EGF) to favour prolonged cell survival, led to a mixed population of both neuronal and glial cells. Instead, the culture conditions I proposed negatively impact on glial cell survival, resulting in a neuronal-enriched culture. In addition, an increasing amount of flat fibroblast-like cells were seen by 4 DIV up to 9 DIV in Patel's work. These cell types were present in irrelevant percentage in my cell cultures, especially around undissociated cell clusters. This high amount of fibroblasts reported by Patel and colleagues could be partially due to a poor efficient dissociation method, as suggested by big cell clusters reported in 1 DIV bright field images. Finally, in agreement with authors observations, I found that cell showed an increasing clustering tendency over time. Protein level analysis revealed that mutant brain-derived neuronal cells exhibited higher Dcc levels with respect to controls only by 2 DIV and not at earlier time points (6 HIV). This result suggested that Dcc upregulation might not be an intrinsic feature but rather a phenomenon evolving over time. Moreover, 2 DIV immunofluorescence showed that a Dcc-positive signal was detectable in discrete spots in mutant brain-derived neurons thus indicating that the Dcc increase could be related to some specific compartments.

Fractional precipitation analysis of mutant head protein lysates showed that Dcc was mainly colocalizing with p62/LC3B-II. On the other hand, wild type lysate subjected to fractionation showed high co-sedimentation of Dcc/LC3B-II together with Lamp1/Rab7. By searching through the literature, I was not able to find any fractional precipitation performed on zebrafish-derived protein lysates; therefore, the pipeline I optimized was the first zebrafish-adapted one. p62/LC3B-II high levels found in Dcc-enriched fraction might indicate that Dcc can be targeted to the autophagic pathway. In agreement with these findings, recent evidence showed that autophagy, and in particular selective autophagy, can be used to modulate signaling pathways and transmembrane receptors (Coelho et al., 2022). This is the case, for example, of the TNF receptor Fn14 which turnover has been demonstrated associated both with the late endosomal and autophagic routes

(Winer et al., 2018). In addition, if considered together with the low levels of Lamp1/Rab7, this might be due to defects in lysosomal receptor targeting in *ids* mutants. This hypothesis was reinforced by findings on 2 DIV primary neuronal cell cultures: indeed, I documented a decrease of lysotracker-positive lysosomes followed by increased Rab7 protein levels in mutant neuronal cell culture when compared to controls. In this context, it has been shown that deficiency in lysosomal acidification induce accumulation of Rab7-positive vesicles in the endo-lysosomal pathway (Minami et al., 2022). In line with these findings, it is well established that altered vesicle trafficking and membrane composition represent a pathological feature of MPSs (Rappaport et al., 2016; Teixeira et al., 2014). Further analysis will allow to directly link Dcc accumulation and lysosomal dysfunction.

Together with receptor transport, I also explored Dcc-related downstream pathway activation. No differences were reported in total brain lysates (2-3 dpf) in pFak/Fak ratio between wild type and *ids* mutants. However, it should be noted that both forms of focal adhesion kinases (Faks) were significantly upregulated in mutant-derived brains. Kinases upregulation was maintained at 6 HIV in brain-derived cell culture; on the other hand, *ids*-derived primary neurons at 2 DIV displayed only pFak and not total Fak upregulation, indicating an overactivation of Fak autophosphorylation. This might suggest that other cell types beyond neurons were responsible for total Fak dysregulation. Indeed, it has been reported that MPS IIIB mouse-derived astrocytes constitutively activate focal adhesions when compared to controls (Bruyère et al., 2015). Accordingly, at 6 HIV the primary culture I was harvesting was probably composed by a mixed population that accounted for a glial component, as seen also at 1 DIV. On the other hand, Fak levels *in vitro* could be influenced by coating composition and consequent cell adhesion capability. Concerning N-Wasp protein levels, differences between genotypes were reported only at 6 HIV and 6 dpf. At 6 HIV, N-Wasp upregulation displayed by mutant-derived cell cultures might be indicative of abnormal cytoskeleton rearrangements during the first steps of cell polarization and axon elongation. The opposite situation was reported, instead, in 6 dpf total brain

lysates. However, analysis of total N-Wasp might not be sufficiently informative; indeed, immunoprecipitation assays are planned to understand whether N-Wasp could be effectively recruited on Dcc luminal side and mediate downstream cytoskeletal rearrangements.

Furthermore, 2 DIV mutant-derived primary cell cultures, grown on dedicated microfluidic devices, showed shorter and more branched processes with respect to controls. Since no zebrafish-adapted protocols were available, this is the first time zebrafish neuronal cells were applied to microfluidic devices. According to the reduced axonal length measured in mutant neurons, I hypothesize that cytoskeletal defects might be implied in incorrect axonal outgrowth. Indeed, recent evidence showed that MPS IIIB mouse brains displayed altered levels in proteins involved in cytoskeleton organization (De Pasquale et al., 2020). Further analyses will be required to dissect the molecular mechanisms underlying the axonal phenotype of mutant-derived cells.

Lysosomal HS engorgement has traditionally been identified as the MPS pathological hallmark; however, when looking at HS total levels I was not able to identify any significant differences between wild type and mutant *ids* larval heads. Although more sophisticated analyses will be required, my preliminary data suggested that the alterations I observed in Dcc levels, downstream pathway and trafficking may not be directly driven by HS accumulation. Indeed, increasing evidence highlights that beyond the mere “substrate accumulation”, HS imbalance and lysosomal dysfunction can have a huge impact also on vesicle trafficking, autophagy and signaling pathways (Fiorenza et al., 2018). Furthermore, HS staining revealed choroid plexus architecture (ChP) as very disorganized in 6 dpf mutant brains with respect to wild type. This structure, mainly formed by polarized epithelial cells, functions as a barrier between cerebrospinal fluid and capillaries. ChP is also directly involved in cerebrospinal fluid secretion thus regulating CNS homeostasis (Henson et al., 2014). ChP alterations have been associated to neurological disorders such as Alzheimer’s disease (Gião et al., 2022) and some cases of LSDs such as Fabry’s disease (Kaye et al., 1988), Niemann-Pick type C (Van Hoecke et al., 2021) and MPS IIIA (Viana et al., 2020). Moreover, defects in ChP

homeostasis are related to hydrocephalus, which is one of the common features shown by MPS II patients, thus underling a possible link between ChP architecture and MPS II pathogenesis that might be investigated in the future.

Protein level analysis on adult dissected brains (3 months old and 2 years old) showed that the Dcc upregulation in *ids* mutants was not temporally restricted to the developmental stages but was consistently present also during adulthood. This might be due to the progressive exacerbation of lysosomal dysfunction with impaired vesicle fusion, resulting in a defective degradative pathway. A block of the autophagic pathway has been reported, for example, both in multiple sulphatase deficiency and MPS IIIA (Settembre et al., 2008).

At these life stages, and even before at 1month of age, mutant fish-derived brains also displayed increased Gfap protein levels when compared to controls. This indicated that glial activation is a very early phenomenon in the zebrafish MPS II model. The same feature, even if delayed to 6 weeks of age, was also recapitulated by the MPS II mouse model (Zalfa et al., 2016). Future investigations will allow to understand which could be the causes leading to glial activation. Since lysosomal defects involve both neurons and astrocytes, it might be that concurrent neuronal and glial degeneration reflects into an auto-sustained phenomenon. Moreover, Dcc accumulation and defects in protein degradation could impact on mitochondria function and oxidative stress. Evaluation of neuronal death, proinflammatory cytokines and reactive oxygen species will allow to dissect the pathological aspects of astrocyte activation. In addition, BBB leakage has been reported in MPS IIIA and MPS IIID patients, suggesting another possible cause for neuroinflammation (Garbuzova-Davis et al., 2013).

Finally, no gross differences between wild type and mutant larvae were reported in the analysis of retinotopic mapping. This suggested that no macroscopical anatomical alterations were present in the visual system. Moreover, investigation of visual stimuli integration showed that mutant larvae responded with the same behaviour regardless of the provided input. No differences between genotypes were also shown in anxiety behaviours induced by dark and light alternation. Even if not significant al larval stages, the possible alterations caused by progressive

phenotypic worsening could impinge on behaviour at later time stages. This is in line with the MPS II mouse model showing anxiety-related behaviours only by 36 weeks of age (Cardone et al., 2006). In addition, recent findings on MPS IIIA zebrafish model showed that, even if a hyperactive phenotype could be traced since larval stages, behavioural abnormalities exacerbated over time (Douek et al., 2021). In the end, since no evidence is reported by the literature, this can be considered the first attempt to behaviourally characterize an MPS II zebrafish model.

Taken altogether, this study provides increasing evidence about the correlation between axon pathfinding and lysosomes in the pathological context of LSDs, as reported for Batten disease (Chu-LaGraff et al., 2010), MPS VII (Parente et al., 2012) and Neuronal ceroid lipofuscinosis 1 (CLN1) (Tikka et al., 2016).

In particular, this thesis proposes that *ids* deficiency impact on AG-related molecules, shedding light on an early pathological mechanism in MPS II onset. Interestingly, as no evident HS accumulation was reported at the time point in which mutant larvae exhibited an AG-related dysregulation, I may conclude that aberrant phenomena could take place before massive HS storage. During this project new zebrafish-adapted protocols have been optimized, such as fractional precipitation, neuronal primary cell culture and microfluidics. Finally, a time course analysis of Gfap protein levels revealed astrocyte activation since the zebrafish juvenile stage, indicating early brain dyshomeostasis. Future investigations will be needed to directly correlate Dcc dysregulation with altered lysosomal degradation and to explore the causes underling glial activation.

BIBLIOGRAPHY

Acosta JR, Watchon M, Yuan KC, Fifita JA, Svahn AJ, Don EK, Winnick CG, Blair IP, Nicholson GA, Cole NJ, Goldsbury C, Laird AS (2018) Neuronal cell culture from transgenic zebrafish models of neurodegenerative disease. Biol Open 7:bio036475.

Adams MM, Kafaligonul H (2018) zebrafish-A Model Organism for Studying the Neurobiological Mechanisms Underlying Cognitive Brain Aging and Use of Potential Interventions. Front Cell Dev Biol 6:135.

Barone R, Pellico A, Pittalà A, Gasperini S (2018) Neurobehavioral phenotypes of neuronopathic mucopolysaccharidoses. Ital J Pediatr 44:121.

Barresi MJF, Hutson LD, Chien C-B, Karlstrom RO (2005) Hedgehog regulated Slit expression determines commissure and glial cell position in the zebrafish forebrain. Development 132:3643–3656.

Bellesso S, Salvalaio M, Lualdi S, Tognon E, Costa R, Braghetta P, Giraudo C, Stramare R, Rigon L, Filocamo M, Tomanin R, Moro E (2018) FGF signaling deregulation is associated with early developmental skeletal defects in animal models for mucopolysaccharidosis type II (MPSII). Hum Mol Genet 27:2407.

Bin JM, Han D, Lai Wing Sun K, Croteau L-P, Dumontier E, Cloutier J-F, Kania A, Kennedy TE (2015) Complete Loss of Netrin-1 Results in Embryonic Lethality and Severe Axon Guidance Defects without Increased Neural Cell Death. Cell Rep 12:1099–1106.

Blanchette CR, Perrat PN, Thackeray A, Bénard CY (2015) Glypican Is a Modulator of Netrin-Mediated Axon Guidance. PLoS Biol 13:e1002183.

Bollmann JH (2019) The zebrafish Visual System: From Circuits to Behavior. Annu Rev Vis Sci 5:269–293.

Bosch ME, Kielian T (2015) Neuroinflammatory paradigms in lysosomal storage diseases. Front Neurosci 9:417.

Bosserhoff A-K, Hofmeister S, Ruedel A, Schubert T (2014) DCC is expressed in a CD166-positive subpopulation of chondrocytes in human osteoarthritic cartilage and modulates CRE activity. Int J Clin Exp Pathol 7:1947–1956.

Bouchard J-F, Moore SW, Tritsch NX, Roux PP, Shekarabi M, Barker PA, Kennedy TE (2004) Protein kinase A activation promotes plasma membrane insertion of DCC from an intracellular pool: A novel mechanism regulating commissural axon extension. J Neurosci 24:3040–3050.

Boulanger-Weill J, Sumbre G (2019) Functional Integration of Newborn Neurons in the zebrafish Optic Tectum. Front Cell Dev Biol 7:57.

Boyer NP, Gupton SL (2018) Revisiting Netrin-1: One Who Guides (Axons). Front Cell Neurosci 12:221.

Bruyère J, Roy E, Ausseil J, Lemonnier T, Teyre G, Bohl D, Etienne-Manneville S, Lortat-Jacob H, Heard JM, Vitry S (2015) Heparan sulfate saccharides modify focal adhesions: implication in mucopolysaccharidosis neuropathophysiology. J Mol Biol 427:775–791.

Campbell DS, Holt CE (2003) Apoptotic pathway and MAPKs differentially regulate chemotropic responses of retinal growth cones. Neuron 37:939–952.

Cardone M, Polito VA, Pepe S, Mann L, D'Azzo A, Auricchio A, Ballabio A, Cosma MP (2006) Correction of Hunter syndrome in the MPSII mouse model by AAV2/8-mediated gene delivery. Hum Mol Genet 15:1225–1236.

Carpentieri JA, Di Cicco A, Lampic M, Andreau D, Del Maestro L, El Marjou F, Coquand L, Bahi-Buisson N, Brault J-B, Baffet AD (2022) Endosomal trafficking defects alter neural progenitor proliferation and cause microcephaly. Nat Commun 13:16.

Casari A, Schiavone M, Facchinello N, Vettori A, Meyer D, Tiso N, Moro E, Argenton F (2014) A Smad3 transgenic reporter reveals TGF-beta control of zebrafish spinal cord development. Developmental Biology 396:81–93.

Chen Z, Lee H, Henle S, Cheever T, Ekker S, Henley J (2013) Primary neuron culture for nerve growth and axon guidance studies in zebrafish (Danio rerio). PloS one 8.

Cheng HJ, Nakamoto M, Bergemann AD, Flanagan JG (1995) Complementary gradients in expression and binding of ELF-1 and Mek4 in development of the topographic retinotectal projection map. Cell 82:371–381.

Cho JY, Chak K, Andreone BJ, Wooley JR, Kolodkin AL (2012) The extracellular matrix proteoglycan perlecan facilitates transmembrane semaphorin-mediated repulsive guidance. Genes Dev 26:2222–2235.

Chu-LaGraff Q, Blanchette C, O'Hern P, Denefrio C (2010) The Batten disease Palmitoyl Protein Thioesterase 1 gene regulates neural specification and axon connectivity during Drosophila embryonic development. PLoS One 5:e14402.

Coelho PP, Hesketh GG, Pedersen A, Kuzmin E, Fortier A-MN, Bell ES, Ratcliffe CDH, Gingras A-C, Park M (2022) Endosomal LC3C-pathway selectively targets plasma membrane cargo for autophagic degradation. Nat Commun 13:3812.

Corrêa T, Poswar F, Santos-Rebouças CB (2022) Convergent molecular mechanisms underlying cognitive impairment in mucopolysaccharidosis type II. Metab Brain Dis 37:2089–2102.

Costa R, Urbani A, Salvalaio M, Bellesso S, Cieri D, Zancan I, Filocamo M, Bonaldo P, Szabò I, Tomanin R, Moro E (2017) Perturbations in cell signaling elicit early cardiac defects in mucopolysaccharidosis type II. Hum Mol Genet 26:1643–1655.

Dang P, Barnes DT, Cheng RP, Xu A, Moon YJ, Kodukula SS, Raper JA (2022) Netrins and Netrin Receptors are Essential for Normal Targeting of Sensory Axons in the zebrafish Olfactory Bulb. Neuroscience S0306-4522(22)00407–9.

De Pasquale V, Costanzo M, Siciliano RA, Mazzeo MF, Pistorio V, Bianchi L, Marchese E, Ruoppolo M, Pavone LM, Caterino M (2020) Proteomic Analysis of Mucopolysaccharidosis IIIB Mouse Brain. Biomolecules 10:355.

De Pasquale V, Pavone LM (2019) Heparan sulfate proteoglycans: The sweet side of development turns sour in mucopolysaccharidoses. Biochim Biophys Acta Mol Basis Dis 1865:165539.

De Risi M et al. (2021) Altered heparan sulfate metabolism during development triggers dopamine-dependent autistic-behaviours in models of lysosomal storage disorders. Nat Commun 12:3495.

Deiner MS, Kennedy TE, Fazeli A, Serafini T, Tessier-Lavigne M, Sretavan DW (1997) Netrin-1 and DCC mediate axon guidance locally at the optic disc: loss of function leads to optic nerve hypoplasia. Neuron 19:575–589.

Douek AM, Amiri Khabooshan M, Henry J, Stamatis S-A, Kreuder F, Ramm G, Änkö M-L, Wlodkowic D, Kaslin J (2021) An Engineered sgsh Mutant zebrafish Recapitulates Molecular and Behavioural Pathobiology of Sanfilippo Syndrome A/MPS IIIA. Int J Mol Sci 22:5948.

Dun X-P, Parkinson DB (2017) Role of Netrin-1 Signaling in Nerve Regeneration. Int J Mol Sci 18:491.

Eisengart JB, King KE, Shapiro EG, Whitley CB, Muenzer J (2020) The nature and impact of neurobehavioral symptoms in neuronopathic Hunter syndrome. Mol Genet Metab Rep 22:100549.

Ellezam B, Selles-Navarro I, Manitt C, Kennedy TE, McKerracher L (2001) Expression of netrin-1 and its receptors DCC and UNC-5H2 after axotomy and during regeneration of adult rat retinal ganglion cells. Exp Neurol 168:105–115.

Fazeli A, Dickinson SL, Hermiston ML, Tighe RV, Steen RG, Small CG, Stoeckli ET, Keino-Masu K, Masu M, Rayburn H, Simons J, Bronson RT, Gordon JI, Tessier-Lavigne M, Weinberg RA (1997) Phenotype of mice lacking functional Deleted in colorectal cancer (Dcc) gene. Nature 386:796–804.

Fecarotta S, Tarallo A, Damiano C, Minopoli N, Parenti G (2020) Pathogenesis of Mucopolysaccharidoses, an Update. Int J Mol Sci 21:2515.

Finci LI, Krüger N, Sun X, Zhang J, Chegkazi M, Wu Y, Schenk G, Mertens HDT, Svergun DI, Zhang Y, Wang J-H, Meijers R (2014) The crystal structure of netrin-1 in complex with DCC reveals the bifunctionality of netrin-1 as a guidance cue. Neuron 83:839–849.

Fiorenza MT, Moro E, Erickson RP (2018) The pathogenesis of lysosomal storage disorders: beyond the engorgement of lysosomes to abnormal development and neuroinflammation. Hum Mol Genet 27:R119–R129.

Förster D, Helmbrecht TO, Mearns DS, Jordan L, Mokayes N, Baier H (2020) Retinotectal circuitry of larval zebrafish is adapted to detection and pursuit of prey. Elife 9:e58596.

Fukuhara N, Howitt JA, Hussain S-A, Hohenester E (2008) Structural and functional analysis of slit and heparin binding to immunoglobulin-like domains 1 and 2 of Drosophila Robo. J Biol Chem 283:16226–16234.

Garbuzova-Davis S, Mirtyl S, Sallot SA, Hernandez-Ontiveros DG, Haller E, Sanberg PR (2013) Blood-brain barrier impairment in MPS III patients. BMC Neurol. 13:174.

Garcia AR, Pan J, Lamsa JC, Muenzer J (2007) The characterization of a murine model of mucopolysaccharidosis II (Hunter syndrome). J Inherit Metab Dis 30:924–934.

Gebhardt C, Auer TO, Henriques PM, Rajan G, Duroure K, Bianco IH, Del Bene F (2019) An interhemispheric neural circuit allowing binocular integration in the optic tectum. Nat Commun 10:5471.

Gião T, Teixeira T, Almeida MR, Cardoso I (2022) Choroid Plexus in Alzheimer's Disease-The Current State of Knowledge. Biomedicines 10:224.

Gleitz HFE, O'Leary C, Holley RJ, Bigger BW (2017) Identification of age-dependent motor and neuropsychological behavioural abnormalities in a mouse model of Mucopolysaccharidosis Type II. PLoS One 12:e0172435.

Harpaz R, Aspiras AC, Chambule S, Tseng S, Bind M-A, Engert F, Fishman MC, Bahl A (2021) Collective behavior emerges from genetically controlled simple behavioral motifs in Zebrafish. Sci Adv 7:eabi7460.

Haynes EM, Ulland TK, Eliceiri KW (2022) A Model of Discovery: The Role of Imaging Established and Emerging Non-mammalian Models in Neuroscience. Frontiers in Molecular Neuroscience 15.

Hedgecock EM, Culotti JG, Hall DH (1990) The unc-5, unc-6, and unc-40 genes guide circumferential migrations of pioneer axons and mesodermal cells on the epidermis in C. elegans. Neuron 4:61–85.

Henriques PM, Rahman N, Jackson SE, Bianco IH (2019) Nucleus Isthmi Is Required to Sustain Target Pursuit during Visually Guided Prey-Catching. Curr Biol. 29(11):1771-1786.

Henson HE, Parupalli C, Ju B, Taylor MR (2014) Functional and genetic analysis of choroid plexus development in zebrafish. Front Neurosci. 8:364.

Hinderer C, Katz N, Louboutin J-P, Bell P, Yu H, Nayal M, Kozarsky K, O'Brien WT, Goode T, Wilson JM (2016) Delivery of an Adeno-Associated Virus Vector into Cerebrospinal Fluid Attenuates Central Nervous System Disease in Mucopolysaccharidosis Type II Mice. Hum Gene Ther 27:906–915.

Hjorth JT, Gad J, Cooper H, Key B (2001) A zebrafish homologue of deleted in colorectal cancer (zdcc) is expressed in the first neuronal clusters of the developing brain. Mech Dev 109:105–109.

Horn KE, Glasgow SD, Gobert D, Bull S-J, Luk T, Girgis J, Tremblay M-E, McEachern D, Bouchard J-F, Haber M, Hamel E, Krimpenfort P, Murai KK, Berns A, Doucet G, Chapman CA, Ruthazer ES, Kennedy TE (2013) DCC expression by neurons regulates synaptic plasticity in the adult brain. Cell Rep 3:173–185.

Jain RA, Bell H, Lim A, Chien C-B, Granato M (2014) Mirror movement-like defects in startle behavior of zebrafish dcc mutants are caused by aberrant midline guidance of identified descending hindbrain neurons. J Neurosci 34:2898–2909.

Jasmin M, Ahn EH, Voutilainen MH, Fombonne J, Guix C, Viljakainen T, Kang SS, Yu L-Y, Saarma M, Mehlen P, Ye K (2021) Netrin-1 and its receptor DCC modulate survival and death of dopamine neurons and Parkinson's disease features. EMBO J 40:e105537.

Junge HJ, Yung AR, Goodrich LV, Chen Z (2016) Netrin1/DCC signaling promotes neuronal migration in the dorsal spinal cord. Neural Dev 11:19.

Jurisch-Yaksi N, Yaksi E, Kizil C (2020) Radial glia in the zebrafish brain: Functional, structural, and physiological comparison with the mammalian glia. Glia 68:2451–2470.

Kastenhuber E, Kern U, Bonkowsky JL, Chien C-B, Driever W, Schweitzer J (2009) Netrin-DCC, Robo-Slit, and heparan sulfate proteoglycans coordinate lateral positioning of longitudinal dopaminergic diencephalospinal axons. J Neurosci 29:8914–8926.

Kaye EM, Kolodny EH, Logigian EL, Ullman MD (1988) Nervous system involvement in Fabry's disease: clinicopathological and biochemical correlation. Ann Neurol 23:505–509.

Keating DJ, Winter MA, Hemsley KM, Mackenzie KD, Teo EH, Hopwood JJ, Brooks DA, Parkinson-Lawrence EJ (2012) Exocytosis is impaired in mucopolysaccharidosis IIIA mouse chromaffin cells. Neuroscience 227:110–118.

Konopacki FA, Wong HH-W, Dwivedy A, Bellon A, Blower MD, Holt CE (2016) ESCRT-II controls retinal axon growth by regulating DCC receptor levels and local protein synthesis. Open Biol 6:150218.

Lai Wing Sun K, Correia JP, Kennedy TE (2011) Netrins: versatile extracellular cues with diverse functions. Development 138:2153–2169.

Lamb CA, Dooley HC, Tooze SA (2013) Endocytosis and autophagy: Shared machinery for degradation. Bioessays 35:34–45.

Lauderdale JD, Davis NM, Kuwada JY (1997) Axon tracts correlate with netrin-1a expression in the zebrafish embryo. Mol Cell Neurosci 9:293–313.

Lee J-S, Chien C-B (2004) When sugars guide axons: insights from heparan sulphate proteoglycan mutants. Nat Rev Genet 5:923–935.

Li W, Lee J, Vikis H, Lee SH, Liu G, Aurandt J, Shen TL, Fearon ER, Guan JL, Han M, Rao Y, Hong K, Guan KL (2004) Activation of FAK and Src are receptor-proximal events required for netrin signaling. Nature neuroscience 7.

Lin L, Lesnick TG, Maraganore DM, Isacson O (2009) Axon guidance and synaptic maintenance: preclinical markers for neurodegenerative disease and therapeutics. Trends Neurosci 32:142–149.

Liu J, Baraban SC (2019) Network Properties Revealed during Multi-Scale Calcium Imaging of Seizure Activity in zebrafish. eNeuro 6:ENEURO.0041-19.2019.

Ma W, Shang Y, Wei Z, Wen W, Wang W, Zhang M (2010) Phosphorylation of DCC by ERK2 is facilitated by direct docking of the receptor P1 domain to the kinase. Structure 18:1502–1511.

Manzoli R, Badenetti L, Rubin M, Moro E (2021) Lysosomal Function and Axon Guidance: Is There a Meaningful Liaison? Biomolecules 11:191.

Meade ME, Roginsky JE, Schulz JR (2019) Primary cell culture of adult zebrafish spinal neurons for electrophysiological studies. J Neurosci Methods 322:50–57.

Mehlen P, Rabizadeh S, Snipas SJ, Assa-Munt N, Salvesen GS, Bredesen DE (1998) The DCC gene product induces apoptosis by a mechanism requiring receptor proteolysis. Nature 395:801–804.

Minami K, Morimoto H, Morioka H, Imakiire A, Kinoshita M, Yamamoto R, Hirato T, Sonoda H (2022) Pathogenic Roles of Heparan Sulfate and Its Use as a Biomarker in Mucopolysaccharidoses. International journal of molecular sciences, 23(19), 11724.

Ming G, Song H, Berninger B, Inagaki N, Tessier-Lavigne M, Poo M (1999) Phospholipase C-gamma and phosphoinositide 3-kinase mediate cytoplasmic signaling in nerve growth cone guidance. Neuron 23:139–148.

Monnier PP, Sierra A, Macchi P, Deitinghoff L, Andersen JS, Mann M, Flad M, Hornberger MR, Stahl B, Bonhoeffer F, Mueller BK (2002) RGM is a repulsive guidance molecule for retinal axons. Nature 419:392–395.

Morimoto H, Morioka H, Imakiire A, Yamamoto R, Hirato T, Sonoda H, Minami K (2022) Dose-dependent effects of a brain-penetrating iduronate-2-sulfatase on neurobehavioral impairments in mucopolysaccharidosis II mice. Mol Ther Methods Clin Dev 25:534–544.

Moro E, Tomanin R, Friso A, Modena N, Tiso N, Scarpa M, Argenton F (2010) A novel functional role of iduronate-2-sulfatase in zebrafish early development. Matrix Biol 29:43–50.

Motas S, Haurigot V, Garcia M, Marcó S, Ribera A, Roca C, Sánchez X, Sánchez V, Molas M, Bertolin J, Maggioni L, León X, Ruberte J, Bosch F (2016) CNS-directed gene therapy for the treatment of neurologic and somatic mucopolysaccharidosis type II (Hunter syndrome). JCI Insight 1:e86696.

Muenzer J, Fu H. (1999) Targeting disruption of the mouse iduronate sulfatase gene. Am J Genet, 65, A427.

Myerowitz R, Puertollano R, Raben N (2021) Impaired autophagy: The collateral damage of lysosomal storage disorders. EBioMedicine 63:103166.

Nagase H, Higashi SL, Iweka CA, Pearson CS, Hirata Y, Geller HM, Katagiri Y (2021) Reliable and sensitive detection of glycosaminoglycan chains with immunoblots. Glycobiology 31:116–125.

O'Donnell M, Chance RK, Bashaw GJ (2009) Axon growth and guidance: receptor regulation and signal transduction. Annu Rev Neurosci 32:383–412.

Palmucci S, Attinà G, Lanza ML, Belfiore G, Cappello G, Foti PV, Milone P, Di Bella D, Barone R, Fiumara A, Sorge G, Ettorre GC (2013) Imaging findings of mucopolysaccharidoses: a pictorial review. Insights Imaging 4:443–459.

Parente MK, Rozen R, Cearley CN, Wolfe JH (2012) Dysregulation of gene expression in a lysosomal storage disease varies between brain regions implicating unexpected mechanisms of neuropathology. PLoS One 7(3):e32419.

Parenti G (2009) Treating lysosomal storage diseases with pharmacological chaperones: from concept to clinics. EMBO Mol Med 1:268–279.

Pasterkamp RJ, Burk K (2021) Axon guidance receptors: Endocytosis, trafficking and downstream signaling from endosomes. Prog Neurobiol 198:101916.

Pasterkamp RJ, Peschon JJ, Spriggs MK, Kolodkin AL (2003) Semaphorin 7A promotes axon outgrowth through integrins and MAPKs. Nature 424:398–405.

Patel BB, Clark KL, Kozik EM, Dash L, Kuhlman JA, Sakaguchi DS (2019) Isolation and culture of primary embryonic zebrafish neural tissue. J Neurosci Methods 328:108419.

Plooster M, Menon S, Winkle CC, Urbina FL, Monkiewicz C, Phend KD, Weinberg RJ, Gupton SL (2017) TRIM9-dependent ubiquitination of DCC constrains kinase signaling, exocytosis, and axon branching. Mol Biol Cell 28:2374–2385.

Polito VA, Cosma MP (2009) IDS crossing of the blood-brain barrier corrects CNS defects in MPSII mice. Am J Hum Genet 85:296–301.

Rajasekharan S, Kennedy TE (2009) The netrin protein family. Genome Biol 10:239.

Rappaport J, Manthe RL, Solomon M, Garnacho C, Muro S (2016) A Comparative Study on the Alterations of Endocytic Pathways in Multiple Lysosomal Storage Disorders. Mol Pharm 13:357–368.

Ren X-R, Ming G-L, Xie Y, Hong Y, Sun D-M, Zhao Z-Q, Feng Z, Wang Q, Shim S, Chen Z-F, Song H-J, Mei L, Xiong W-C (2004) Focal adhesion kinase in netrin-1 signaling. Nat Neurosci 7:1204–1212.

Rigby MJ, Gomez TM, Puglielli L (2020) Glial Cell-Axonal Growth Cone Interactions in Neurodevelopment and Regeneration. Front Neurosci 14:203.

Robertson CE, Martin A, Baker CI, Baron-Cohen S (2012) Atypical integration of motion signals in Autism Spectrum Conditions. PLoS One 7:e48173.

Rock S, Rodenburg F, Schaaf MJM, Tudorache C (2022) Detailed Analysis of zebrafish Larval Behaviour in the Light Dark Challenge Assay Shows That Diel Hatching Time Determines Individual Variation. Front Physiol 13:827282.

Rosenberg AF, Isaacman-Beck J, Franzini-Armstrong C, Granato M (2014) Schwann cells and deleted in colorectal carcinoma direct regenerating motor axons towards their original path. J Neurosci 34:14668–14681.

Russo G, Lehne F, Pose Méndez SM, Dübel S, Köster RW, Sassen WA (2018) Culture and Transfection of zebrafish Primary Cells. J Vis Exp 57872.

Salvalaio M, D'Avanzo F, Rigon L, Zanetti A, D'Angelo M, Valle G, Scarpa M, Tomanin R (2017) Brain RNA-Seq Profiling of the Mucopolysaccharidosis Type II Mouse Model. Int J Mol Sci 18:1072.

Sepp KJ, Schulte J, Auld VJ (2001) Peripheral glia direct axon guidance across the CNS/PNS transition zone. Dev Biol 238:47–63.

Settembre C, Fraldi A, Jahreiss L, Spampanato C, Venturi C, Medina D, de Pablo R, Tacchetti C, Rubinsztein DC, Ballabio A (2008) A block of autophagy in lysosomal storage disorders. Hum Mol Genet 17:119–129.

Shekarabi M, Moore SW, Tritsch NX, Morris SJ, Bouchard J-F, Kennedy TE (2005) Deleted in colorectal cancer binding netrin-1 mediates cell substrate adhesion and recruits Cdc42, Rac1, Pak1, and N-WASP into an intracellular signaling complex that promotes growth cone expansion. J Neurosci 25:3132–3141.

Smock RG, Meijers R (2018) Roles of glycosaminoglycans as regulators of ligand/receptor complexes. Open Biol 8:180026.

Spilman PR, Corset V, Gorostiza O, Poksay KS, Galvan V, Zhang J, Rao R, Peters-Libeu C, Vincelette J, McGeehan A, Dvorak-Ewell M, Beyer J, Campagna J, Bankiewicz K, Mehlen P, John V, Bredesen DE (2016) Netrin-1 Interrupts Amyloid-β Amplification, Increases sAβPPα in vitro and in vivo, and Improves Cognition in a Mouse Model of Alzheimer's Disease. J Alzheimers Dis 52:223–242.

Štih V, Petrucco L, Kist AM, Portugues R (2019) Stytra: An open-source, integrated system for stimulation, tracking and closed-loop behavioral experiments. PLoS Comput Biol 15:e1006699.

Teixeira CA, Miranda CO, Sousa VF, Santos TE, Malheiro AR, Solomon M, Maegawa GH, Brites P, Sousa MM (2014) Early axonal loss accompanied by impaired endocytosis, abnormal axonal transport, and decreased microtubule stability occur in the model of Krabbe's disease. Neurobiol Dis 66:92–103.

Tikka S, Monogioudi E, Gotsopoulos A, Soliymani R, Pezzini F, Scifo E, Uusi-Rauva K, Tyynelä J, Baumann M, Jalanko A, Simonati A, Lalowski M (2016) Proteomic Profiling in the Brain of CLN1 Disease Model Reveals Affected Functional Modules. Neuromolecular Med 18:109–133.

Tojima T, Kamiguchi H (2015) Exocytic and endocytic membrane trafficking in axon development. Dev Growth Differ 57:291–304.

Vafiadaki E, Cooper A, Heptinstall L, Hatton C, Thornley M, Wraith J (1998) Mutation analysis in 57 unrelated patients with MPS II (Hunter's disease). Arch Dis Child 79:237–241.

Van Hoecke L, Van Cauwenberghe C, Dominko K, Van Imschoot G, Van Wonterghem E, Castelein J, Xie J, Claeys W, Vandendriessche C, Kremer A, Borghgraef P, De Rycke R, Hecimovic S, Vandenbroucke RE (2021) Involvement of the Choroid Plexus in the Pathogenesis of Niemann-Pick Disease Type C. Front Cell Neurosci 15:757482.

Vaz R, Hofmeister W, Lindstrand A (2019) Zebrafish Models of Neurodevelopmental Disorders: Limitations and Benefits of Current Tools and Techniques. Int J Mol Sci 20:1296.

Viana GM, Priestman DA, Platt FM, Khan S, Tomatsu S, Pshezhetsky AV (2020) Brain Pathology in Mucopolysaccharidoses (MPS) Patients with Neurological Forms. J Clin Med 9:396.

Vigouroux RJ, Cesar Q, Chédotal A, Nguyen-Ba-Charvet KT (2020) Revisiting the role of Dcc in visual system development with a novel eye clearing method. Elife 9:e51275.

Vosberg DE, Leyton M, Flores C (2020) The Netrin-1/DCC guidance system: dopamine pathway maturation and psychiatric disorders emerging in adolescence. Mol Psychiatry 25:297–307.

Wilhelmsson U, Bushong EA, Price DL, Smarr BL, Phung V, Terada M, Ellisman MH, Pekny M (2006) Redefining the concept of reactive astrocytes as cells that remain within their unique domains upon reaction to injury. Proc Natl Acad Sci U S A 103:17513–17518.

Wilkerson MJ, Lewis DC, Marks SL, Prieur DJ (1998) Clinical and morphologic features of mucopolysaccharidosis type II in a dog: naturally occurring model of Hunter syndrome. Vet Pathol 35:230–233.

Winer H, Fraiberg M, Abada A, Dadosh T, Tamim-Yecheskel B-C, Elazar Z (2018) Autophagy differentially regulates TNF receptor Fn14 by distinct mammalian Atg8 proteins. Nat Commun 9:3744.

Xie Y, Hong Y, Ma X-Y, Ren X-R, Ackerman S, Mei L, Xiong W-C (2006) DCC-dependent phospholipase C signaling in netrin-1-induced neurite elongation. J Biol Chem 281:2605–2611.

Xu B, Goldman JS, Rymar VV, Forget C, Lo PS, Bull SJ, Vereker E, Barker PA, Trudeau LE, Sadikot AF, Kennedy TE (2010) Critical roles for the netrin receptor deleted in colorectal cancer in dopaminergic neuronal precursor migration, axon guidance, and axon arborization. Neuroscience 169:932–949.

Xu S, Liu Yiqiong, Li X, Liu Ying, Meijers R, Zhang Y, Wang J-H (2018) The binding of DCC-P3 motif and FAK-FAT domain mediates the initial step of netrin-1/DCC signaling for axon attraction. Cell Discov 4:8.

Zalfa C, Verpelli C, D'Avanzo F, Tomanin R, Vicidomini C, Cajola L, Manara R, Sala C, Scarpa M, Vescovi AL, De Filippis L (2016) Glial degeneration with oxidative damage drives neuronal demise in MPSII disease. Cell Death Dis 7:e2331.

Zhang C, Gao J, Zhang H, Sun L, Peng G (2012) Robo2--slit and Dcc--netrin1 coordinate neuron axonal pathfinding within the embryonic axon tracts. J Neurosci 32:12589–12602.